

Supporting Information

Photocatalytic CO₂ Reduction Using a Robust Multifunctional Iridium Complex towards the Selective Formation of Formic Acid

Kenji Kamada,[†] Jieun Jung^{*,†} Taku Wakabayashi,[†] Keita Sekizawa,[‡] Shunsuke Sato,[‡] Takeshi Morikawa,[‡] Shunichi Fukuzumi,[§] and Susumu Saito^{*,†,||}

[†]Department of Chemistry, Graduate School of Science, Nagoya University, Chikusa, Nagoya 464-8602, Japan

[‡]Toyota Central R&D Labs., Inc., 41-1 Yokomichi, Nagakute 480-1192, Japan

[§]Faculty of Science and Engineering, Meijo University, Nagoya 468-8502, Japan

^{||}Research Center for Materials Science (RCMS), Nagoya University, Chikusa, Nagoya 464-8602, Japan.

*To whom correspondence should be addressed.

E-mail: jieun@chem.nagoya-u.ac.jp, saito.susumu@f.mbox.nagoya-u.ac.jp

Experimental Section

Generals. All experiments were performed under an Ar atmosphere unless otherwise noted. ^1H and ^{13}C NMR spectra were recorded on a JEOL ECA-600 (600 MHz for ^1H , 150 MHz for ^{13}C) at 27 °C. Chemical shifts are reported as δ in ppm and are internally referenced to tetramethylsilane (0.0 ppm for ^1H) and CDCl_3 (77.2 ppm for ^{13}C). The following abbreviations are used: s = singlet, d = doublet, t = triplet, q = quartet, bs = broad singlet, dd = doublet of doublet, and m = multiplet. ^{31}P NMR spectra were measured on JEOL ECA-600 (243 MHz) at ambient temperature unless otherwise noted. Chemical shifts are reported in ppm from the solvent resonance employed as the external standard (phosphoric acid (85 wt% in H_2O) at 0.0 ppm). High-resolution mass spectra (HRMS) were obtained from PE Biosystems QSTAR (ESI). For thin-layer chromatography (TLC) analysis through this work, Merck precoated TLC plates (silica gel 60 GF254 0.25 mm) were used. The products were purified by preparative column chromatography on silica gel 60 N (spherical, neutral) (40 – 100 μm ; Kanto). Density functional theory (DFT) calculations were carried out using Gaussian 09 Rev. B 01.^{S1} The molecular structure and the energy were obtained at the B3LYP level with LANL2DZ with f-type pseudopotentials for Ir; 6-31G** for the other atoms.

Materials. Commercially available chemicals were used without further purification unless otherwise indicated. Methyllithium (3 M in diethoxymethane), diisopropylamine, ferrocene, 1,10-phenanthroline, lithium tetraphenylborate tris (1,2-dimethoxyethane) and carbon- ^{13}C dioxide were purchased from Aldrich Chemical Co. Morpholine, *n*-BuLi (1.6 M in hexane), *N,N*-dimethylacetamide (anhydrous), THF (anhydrous), methanol (anhydrous), diethyl ether (anhydrous), ethyl acetate, chloroform, D_2O and celite were purchased from Kanto Chemicals, Ltd. Borane-tetrahydrofuran complex, triethanolamine, ethanol (anhydrous), chlorodicyclohexylphosphine, chloroform-*d*, mercury and hexane were purchased from FUJIFILM Wako Pure Chemical Corporation. Bromoferrocene, tetraethylammonium tetrafluoroborate, 2,4,6-trimethylphenylboronic acid, 4,4'-dibromo-2,2'-bipyridyl, tetrakis(triphenylphosphine)palladium(0), 1,4-dimethoxybenzene, and 1,2,4-trimethoxybenzene were purchased from Tokyo Chemical Industry CO., Ltd. Chloro(1,5-cyclooctadiene)iridium(I) dimer was purchased from FURUYA METAL CO., LTD. Manganese (IV) dioxide was purchased from Merck. Triphenylamine was pur-

chased from NACALAI TESQUE, INC. Carbon dioxide gas was purchased from Alpha system Co., Ltd. *N,N*-dimethylacetamide-*d*₉ was purchased from Cambridge Isotope Laboratories, Inc. 1,3-dimethyl-2-phenyl-2,3-dihydro-1*H*-benzo[*d*]imidazole (BIH) was synthesized according to the literature.^{S2} 1,2,3,4-tetramethoxybenzene was synthesized according to the literature.^{S3}

Instrumentation. Products obtained in the photocatalytic reduction reactions were analyzed by Micro-GC (Agilent 490) equipped with a thermal conductivity detector (column: MS5A 10-m BF column; isothermal at 80 °C; carrier gas: Ar), and Prominence Organic Acid Analysis System (SCR-102H Column; Column Temp.: 40 °C; Cell Temp.: 43 °C) or ion chromatography (IC) instrument (Dionex ICS-2000) with IonPacAS15 and IonPacAG15 columns. EPR spectra were recorded at 173 K with use of a JEOL X-band spectrometer (JES-FA100). The *g* value was calibrated using the Mn²⁺ marker. The magnitude of modulation was chosen to optimize the resolution and the signal-to-noise (S/N) ratio of the observed spectra. The experimental parameters for EPR measurements by JES-FA100 were as follows: microwave frequency = 9.009 GHz, microwave power = 1.0 mW, modulation amplitude = 20.0 G, modulation frequency = 100 kHz and time constant = 0.03 s. Sub-nanosecond laser-induced transient absorption spectra were collected by a customized measuring system developed by Unisoku Co., Ltd., which is based on a Randomly-Interleaved-Pulse-Train method.^{S4} The pump laser used is a wavelength-tunable picosecond laser, PL-2210A and PG403, EKSPLA, whose pulse width is 25 ps. Cyclic voltammetry (CV) and differential pulse voltammetry (DPV) were carried out in DMA containing 0.10 M tetrabutylammonium tetrafluoroborate (TBABF₄) as an electrolyte at 298 K under Ar with use of a glassy carbon as a working electrode (3.0 mm diameter), a platinum wire as a counter electrode, and a Ag/AgNO₃ reference electrode (in CH₃CN solution containing 0.10 M tetrabutylammonium perchlorate and 0.01 M AgNO₃). The potentials were calibrated by the standard potential of ferrocene/ferrocenium (Fc/Fc⁺). UV-vis spectra were recorded on a Hewlett Packard 8453 diode array spectrophotometer equipped with a UNISOKU Scientific Instruments Cryostat USP-203A.

Kinetic Measurements. The reactions were run in a 1.0 cm quartz cuvette and followed by monitoring transient absorption spectral changes (excited at 355 nm) of the reaction solutions of Mes-IrPCY2 (1.0 mM) in the presence of ferrocene (0.25 – 2.0 mM) in DMA at 298 K. The same

procedure was used for spectral measurements for oxidation of other substrates with Mes-IrPCY2. Second-order rate constants were determined under pseudo-first-order conditions (i.e., [substrate]/[Ir] > 10) by fitting the changes in transient absorbance for the decay of peaks due to the excited Ir complex in the oxidation reactions of substrates (0.25 – 100 mM) in DMA at 298 K. Reactions of the Ir complex with substrates were monitored by the changes in the absorption bands at 500 nm.

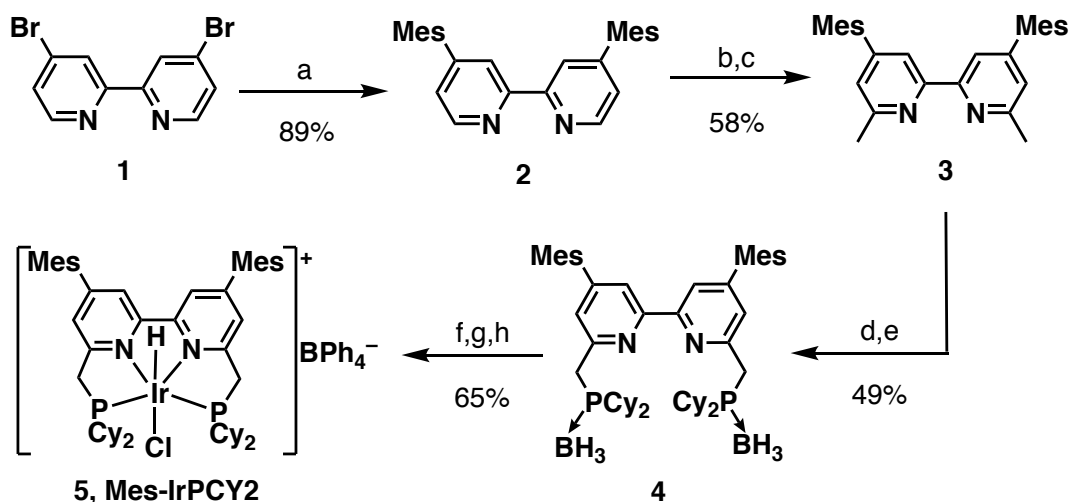
Product analysis. An CO₂-saturated mixture of DMA/H₂O solution of Mes-IrPCY2 and an CO₂-saturated DMA solution of BIH were added to 8.0 mL test tubes under CO₂ to prepare 4.0 mL of a mixture of DMA/H₂O (9:1, v/v; 4.0 mL) containing Mes-IrPCY2 (20 μM) and BIH (0.2 M). The solutions were irradiated in a turntable irradiation apparatus at room temperature using a Xe lamp (300W) combined with a UV-cut filter having a cutoff wavelength of 400 nm and a UV and IR cut filter ranging from 385 nm to 740 nm. The gaseous reaction products were analyzed using a micro-GC (Agilent 490) equipped with a thermal conductivity detector (column: MS5A 10-m BF column; isothermal at 80 °C; carrier gas: Ar), and the products in the solution were analyzed using Prominence Organic Acid Analysis System (SCR-102H Column; Column Temp.: 40 °C; Cell Temp.: 43 °C) or IC instrument (Dionex ICS-2000) with IonPacAS15 and IonPacAG15 columns. The column temperature was maintained at 308 K. A solution of 3.0 mM KOH was used as the first eluent up to 10 min, and then the eluent was changed gradually to 10 mM KOH over 5 min, followed by a change to 30 mM KOH solution over 5 min.

EPR Measurements. Photoirradiation ($\lambda \geq 400$ nm) of a mixture of DMA/H₂O (9:1, v/v; 4.0 mL) containing Mes-IrPCY2 (1.0 mM) and BIH (0.10 M) or a mixture of 9:1:2 DMA/H₂O/TEOA containing Mes-IrPCY2 (1.0 mM) was performed using a 300 W Xenon lamp (ASAHI SPECTRA, MAX-303) for 20 min at 233 K. After the photoirradiation, EPR spectra were recorded at 173 K.

Quantum Yield Determination. A quantum yield (Φ) of photocatalytic reduction of CO₂ in an CO₂-saturated mixture of DMA/H₂O (9:1, v/v; 4.0 mL) containing BIH and Mes-IrPCY2 was determined under visible light irradiation of monochromatized light using a Xe lamp (300 W) on an ASAHI SPECTRA MAX-303 through a band-pass filter transmitting $\lambda = 400$ nm at 298 K. Typically, the amount of HCOOH and CO produced during the photochemical reaction was determined

under photoirradiation ($\lambda = 400$ nm) with irradiation time interval of 2 h (see Figure S3 in SI). The slope of the graph in 0 – 10 h for HCOOH and 2 – 10 h for CO is taken to determine the quantum yield. The quantum yield was determined using the following equation, Φ (%) = $(2 \times R/I) \times 100$, where R (mol s^{-1}) is the rate of formation of CO and HCOOH, and I (einstein s^{-1}) is the rate of photon flux of the incident light. The total number of incident photons was determined using a standard actinometer as follows. A test tube containing an aqueous solution (4.0 mL) of potassium ferrioxalate ($\text{K}_3[\text{Fe}^{\text{III}}(\text{C}_2\text{O}_4)_3]$; 6.0 mM) was irradiated using monochromatized light ($\lambda = 400$ nm) for 1, 2 and 3 min at 298 K. At the end of the irradiation, a sodium acetate buffer solution (2.0 mL) of phenanthroline was added to 1.0 mL of the actinometer solution and the solution was kept under dark for 1 h. The absorbance at 510 nm due to $[\text{Fe}(\text{phen})_3]^{2+}$ ($\epsilon = 11050 \text{ M}^{-1} \text{ cm}^{-1}$ at $\lambda_{\text{max}} = 510$ nm) was measured to determine the total number of incident photons using the quantum yield for the photodecomposition of ferrioxalate ($\Phi = 1.14$ at 405–407 nm)^{S5} to be $2.02 \times 10^{-9} \text{ einstein s}^{-1}$ [rate of formation of $[\text{Fe}(\text{phen})_3]^{2+}$ after dilution = 2.12×10^{-3} (slope of a inset) / 11050 (ϵ) = $1.92 \times 10^{-7} \text{ M s}^{-1}$ and rate of formation of $[\text{Fe}(\text{phen})_3]^{2+}$ before dilution = $1.92 \times 10^{-7} \text{ M s}^{-1} \times (4 \times 10^{-3} \text{ L}) \times 3$ (rate of dilution) = $2.31 \times 10^{-9} \text{ mol s}^{-1}$, $I = 2.31 \times 10^{-9} / 1.14 = 2.02 \times 10^{-9} \text{ einstein s}^{-1}$]. The same measurements were repeated twice more, and the average value of them was $2.00 \times 10^{-9} \text{ einstein s}^{-1}$. Because the percentage of light absorption of actinometer solution is 96.8%, the total number of incident photons is $2.07 \times 10^{-9} \text{ einstein s}^{-1}$ (Figure S3b). The quantum yields of the production of HCOOH and CO were calculated by following equation: QY (%) = $(2 \times R/I) \times 100\%$, where R is the evolution rate of HCOOH ($41 \times 10^{-10} \text{ mol s}^{-1}$) and CO ($7.9 \times 10^{-11} \text{ mol s}^{-1}$) and I is the rate of photon flux irradiated to the reaction mixture ($2.07 \times 10^{-9} \text{ einstein s}^{-1}$). The quantum yields obtained under these conditions were estimated to be $\Phi_{\text{HCOOH}} = 41\%$ and $\Phi_{\text{CO}} = 7.9\%$.

Syntheses



Scheme S1. The synthesis of Mes-IrPCY2 proceeds *via* **1** to **5**. Reagents: a) 2,4,6-trimethylphenylboronic acid, Pd(PPh₃)₄, Ba(OH)₂•8H₂O, 1,4-dioxane, H₂O; b) MeLi, THF; c) MnO₂, CH₂Cl₂; d) LDA, PCy₂Cl, THF; e) BH₃-THF; f) Morpholine; g) [Ir(cod)Cl]₂, MeOH; h) LiBPh₄(glyme)₃, MeOH.

4,4'-Bis(2,4,6-trimethylphenyl)-2,2'-bipyridine (2): This compound was prepared according to the literature procedures^{S6} with small modifications. In a 200 mL two-necked flask equipped with a condenser, 2,4,6-trimethylphenylboronic acid (3.1510 g, 19.2 mmol), barium hydroxide octahydrate (18.8071 g, 60 mmol), tetrakis (triphenyl-phosphine) palladium (1.8469 g, 1.6 mmol), 4,4'-dibromo-2,2'-bipyridine (2.5148 g, 8.0 mmol), anhydrous 1,4-dioxane (75 mL), H₂O (25 mL), and magnetic stirring bar were placed under Ar atmosphere. The reaction mixture was refluxed for 24 hours under nitrogen gas and cooled to room temperature. The solvent was removed and the contents were poured into chloroform. After the precipitate formed was removed by filtration through filter paper, the organic layer was washed with water and brine, and dried over Na₂SO₄. After evaporation of chloroform under a reduced pressure, the resulting residue was diluted with a small quantity of methanol. The precipitate formed was immediately filtrated, dried and purified by column chromatography on silica gel with 9:1 dichloromethane/methanol mixture as eluent and washed with meth-

anol to afford target compound as white solid (2.8002 g, 89% yield). ^1H NMR (600 MHz, CDCl_3): δ 8.70 (d, 2H, $J = 4.8$ Hz, $\text{C}_{10}\text{H}_6\text{N}_2$), 8.32 (m, 2H, $\text{C}_{10}\text{H}_6\text{N}_2$), 7.13 (dd, 2H, $J = 4.8, 1.4$ Hz, $\text{C}_{10}\text{H}_6\text{N}_2$), 6.96 (s, 4H, $\text{C}_6\text{H}_2(\text{CH}_3)_3$), 2.34 (s, 6H, $\text{C}_6\text{H}_2(\text{CH}_3)_3$), 2.05 (s, 12H, $\text{C}_6\text{H}_2(\text{CH}_3)_3$). $^{13}\text{C}\{^1\text{H}\}$ NMR (151 MHz, CDCl_3): δ 156.6, 150.8, 149.6, 137.5, 136.7, 135.3, 128.4, 125.0, 122.3, 21.2, 20.8. HRMS (ESI, $(\text{M}+\text{H})^+$) Calcd for $\text{C}_{28}\text{H}_{29}\text{N}_2^+$: 393.2331. Found: 393.2309. These spectral data were roughly consistent with the reported values.^{S7}

4,4'-Bis(2,4,6-trimethylphenyl)-6,6'-dimethyl-2,2'-bipyridine (3): In a 100 mL two-necked flask, 4,4'-bis(2,4,6-trimethylphenyl)-2,2'-bipyridine (1.9650 g, 5.0 mmol), anhydrous THF (33 mL) and magnetic stirring bar were placed under Ar atmosphere. To the solution was added 3 M methyllithium (6.7 mL, 20 mmol) at -61 °C. The resulting solution was stirred at this temperature for 1 h and then warmed to 0 °C. After overnight at this temperature, the mixture was refluxed 4.5 h at 80 °C. Then pure water was added to the reaction mixture at 0 °C and organic phase was removed *in vacuo*. Following extraction with CH_2Cl_2 (30 mL \times 4), the organic layer was dried with Na_2SO_4 and filtered. To the filtrate was added MnO_2 (13.3 g) at room temperature. After stirring 1.5 h, the mixture was filtered over celite and evaporated. The crude product was purified by column chromatography (SiO_2 , AcOEt:hexane = 1:5) and washed with MeOH to afford target compound as white solid (1.2093 g, 58% yield). ^1H NMR (600 MHz, CDCl_3): δ 8.10 (d, 2H, $J = 1.2$ Hz, $\text{C}_{10}\text{H}_4\text{N}_2$), 6.96 (m, 6H, $\text{C}_{10}\text{H}_4\text{N}_2$, $\text{C}_6\text{H}_2(\text{CH}_3)_3$), 2.62 (s, 6H, CH_3), 2.34 (s, 6H, $\text{C}_6\text{H}_2(\text{CH}_3)_3$), 2.05 (s, 12H, $\text{C}_6\text{H}_2(\text{CH}_3)_3$). $^{13}\text{C}\{^1\text{H}\}$ NMR (151 MHz, CDCl_3): δ 158.3, 156.3, 150.6, 137.4, 137.2, 135.4, 128.4, 124.1, 119.4, 24.9, 21.2, 20.9. HRMS (ESI, $(\text{M}+\text{H})^+$) Calcd for $\text{C}_{30}\text{H}_{33}\text{N}_2^+$: 421.2644. Found: 421.2602.

6,6'-Bis((dicyclohexylphosphino)methyl)-4,4'-bis(2,4,6-trimethylphenyl)-2,2'-bipyridine–diborane Complex (4): In a 200 mL two-necked flask, 4,4'-bis(2,4,6-trimethylphenyl)-2,2'-bipyridine (0.8418 g, 2.0 mmol), anhydrous THF (10 mL) and magnetic stirring bar were placed under Ar atmosphere. The flask was immersed in an ice bath and stirred at 0 °C. To the solution was added LDA (prepared by mixing diisopropylamine (1.7 mL, 12 mmol), *n*-BuLi (1.6 M in hexane, 7.5 mL), and

6.0 mL anhydrous THF for 10 min stirred at 0 °C). The resulting solution was stirred for 1 h at room temperature. To the solution was added chlorodicyclohexylphosphine (0.88 mL, 4.0 mmol) dropwise to the solution at 0 °C. After stirring for 2.5 h at room temperature, to the solution was added BH₃-THF solution (0.9 M in THF, 22.2 mL, 20 mmol). After stirring at room temperature for 9.5 h, the reaction mixture was quenched by 20 mL water at 0 °C, and the organic phase was removed *in vacuo*. After extraction with CHCl₃, the organic layer was dried over Na₂SO₄ and filtered. The solvent was evaporated, and the residue was purified by column chromatography (SiO₂, Hexane: ethyl acetate = 10:1) and washing with ethyl acetate to afford the target compound as white solid (0.8297 g, 49% yield). ¹H NMR (600 MHz, CDCl₃): δ 8.23 (s, 2H, C₁₀H₄N₂), 7.13 (s, 2H, C₁₀H₄N₂), 6.95 (s, 4H, C₆H₂(CH₃)₃), 3.30 (d, 4H, *J* = 10.8 Hz, PCH₂), 2.34 (s, 6H, C₆H₂(CH₃)₃), 2.04 (s, 12H, C₆H₂(CH₃)₃), 1.93–1.62 (m, 23H, C₆H₁₁), 1.37–1.00 (m, 21H, C₆H₁₁), 0.43 (br, 6H, BH₃) ¹³C{¹H} NMR (151 MHz, CDCl₃): δ 155.4, 155.2 (d, ²*J*_{PC} = 11.7 Hz), 151.5, 137.6, 136.5, 135.1, 128.3, 125.9, 119.9, 31.6 (d, ¹*J*_{PC} = 31.9 Hz), 30.6 (d, ¹*J*_{PC} = 26.0 Hz), 27.0 (d, ²*J*_{PC} = 8.8 Hz), 27.0 (d, ²*J*_{PC} = 7.2 Hz), 26.8, 26.7, 26.1, 21.2, 20.8. ³¹P{¹H} NMR (243 MHz, CDCl₃): δ 29.5 (s). HRMS (ESI, (M+H)⁺) Calcd for C₅₄H₈₇B₂N₂P₂⁺: 841.6061. Found: 841.6013.

Mes-IrPCY2 (5): In a vessel equipped with a young stopcock, 6,6'-bis((dicyclohexylphosphino)methyl)-4,4'-bis(2,4,6-trimethylphenyl)-2,2'-bipyridine-diborane complex (0.3373 g, 0.40 mmol), degassed morpholine (12 mL) and magnetic stirring bar were placed under Ar atmosphere. The mixture was stirred at 120 °C in 2 h and cooled to room temperature, before morpholine was removed *in vacuo* (*ca.* 0.1 mmHg, 70 °C). To the residue was added chloro(1,5-cyclooctadiene) iridium(I) dimer (0.1345 g, 0.20 mmol) and degassed methanol (14.4 mL). The resulting mixture was heated at 70 °C for 10 h, and then cooled down to room temperature. After the mixture was filtered through a pad of celite under Ar atmosphere, lithium tetrphenylborate tris(1,2-dimethoxyethane) (0.4773 g, 0.80 mmol) was added to the filtrate to afford yellow precipitation. The suspension was stirred overnight at room temperature. The precipitation was collected by filtration, washed with methanol, and then

dried *in vacuo* to obtain Mes-IrPCY2 as slightly greenish yellow solid (0.3564 g, 65% yield). ^1H NMR (600 MHz, CDCl_3): δ 7.53 (s, 2H, $\text{C}_{10}\text{H}_4\text{N}_2$), 7.36 (br, 8H, $\text{B}(\text{C}_6\text{H}_5)_4$), 7.19 (s, 2H, $\text{C}_{10}\text{H}_4\text{N}_2$), 6.97 (s, 2H, $\text{C}_6\text{H}_2(\text{CH}_3)_3$), 6.92 (m, 10H, $\text{B}(\text{C}_6\text{H}_5)_4$, $\text{C}_6\text{H}_2(\text{CH}_3)_3$), 6.81 (t, 4H, $J = 7.3$ Hz, $\text{B}(\text{C}_6\text{H}_5)_4$), 3.76 (m, 2H, PCH_2), 3.46 (m, 2H, PCH_2), 2.45 (m, 2H, C_6H_{11}), 2.33 (s, 6H, $\text{C}_6\text{H}_2(\text{CH}_3)_3$), 2.22 (m, 2H, C_6H_{11}), 2.03 (s, 6H, $\text{C}_6\text{H}_2(\text{CH}_3)_3$), 1.99–1.70 (br, 20H, $\text{C}_6\text{H}_2(\text{CH}_3)_3$, C_6H_{11}), 1.56–1.47 (br, 8H, C_6H_{11}), 1.32–0.96 (br, 18H, C_6H_{11}), –21.0 (t, 1H, $J = 17.4$ Hz, IrH). $^{13}\text{C}\{^1\text{H}\}$ NMR (151 MHz, CDCl_3): δ 164.8, 164.5, 164.2, 163.8, 161.5, 156.3, 154.1, 139.2, 136.4, 134.9, 134.5, 133.8, 129.0 (d, $^2J_{\text{PC}} = 17.4$ Hz), 125.6, 123.2, 121.8, 39.5 (d, $^1J_{\text{PC}} = 33.2$ Hz), 36.1 (d, $^1J_{\text{PC}} = 34.7$ Hz), 35.7 (d, $^1J_{\text{PC}} = 29.0$ Hz), 29.0, 28.6, 28.3, 27.6, 27.2 (m), 26.5 (m), 26.3 (m), 26.1, 21.3, 21.0, 20.8. $^{31}\text{P}\{^1\text{H}\}$ NMR (243 MHz, CDCl_3): δ 20.7 (s). HRMS (ESI, $(\text{M}-\text{BPh}_4)^+$) Calcd for $\text{C}_{54}\text{H}_{75}\text{N}_2\text{P}_2\text{Ir}^+$: 1041.4723. Found: 1041.4855. Anal. Calcd. for $\text{C}_{78}\text{H}_{95}\text{B}_1\text{Cl}_1\text{Ir}_1\text{N}_2\text{P}_2$: C 68.83, H 7.04, N 2.06, found: C 68.17, H 7.01, N 2.28.

Table S1. Reactivities for Photocatalytic CO₂ Reduction in Control Experiments

	Solution	Hg	TONs in 24 h irradiation		
			HCO ₂ H	CO	H ₂
1	DMA/H ₂ O (9:1, v/v; 4 mL)	0.17 M	291(30)	69(1)	0.9
2	DMA/H ₂ O (9:1, v/v; 4 mL)	–	323(30)	62(4)	0.8
3	DMA (4 mL)	–	188(10)	3.9(0.3)	0.9

^aThe photocatalytic reaction with Mes-IrPCY2 (20 μM) in a CO₂-saturated mixture under photoirradiation ($\lambda \geq 400$ nm) for 24 h at 298 K.

Table S2. One-Electron Oxidation Potentials (E_{ox}) of Reductants and Second-Order Rate Constants of Electron Transfer (k_{et}) from Reductants to the Excited State of Mes-IrPCY2 ($\lambda = 355$ nm) in DMA at 298 K

reductant	E_{ox} , V vs SCE ^a	k_{et} , M ⁻¹ s ⁻¹
1,4-dimethoxybenzene	1.24	2.83×10^7
1,2,3,4-tetramethoxybenzene	1.17	4.90×10^7
1,2,4-trimethoxybenzene	0.74	5.02×10^8
triphenylamine	0.83	9.32×10^8
bromoferrocene	0.54	2.33×10^9
ferrocene	0.37	3.17×10^9

^a One-electron oxidation potentials of reductants were determined by cyclic voltammetry (CV) and differential pulse voltammetry (DPV) in DMA containing 0.10 M of TBABF₄ at 298 K.

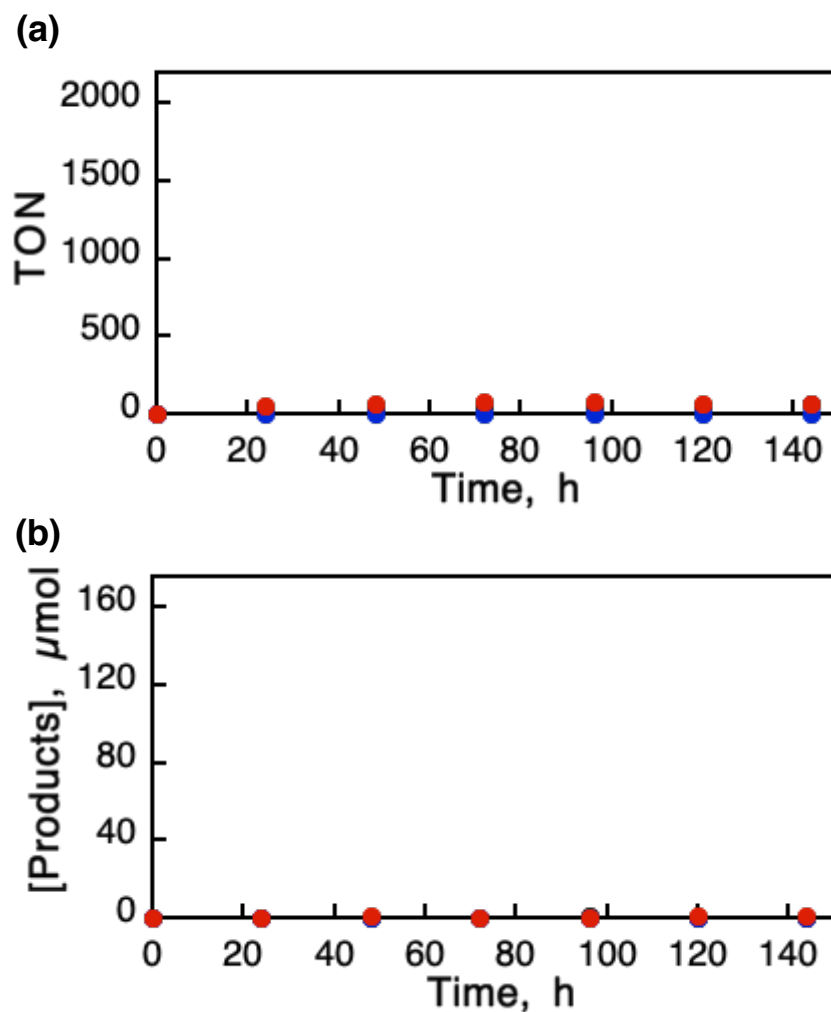


Figure S1. Time courses of formation of HCOOH (red), CO (blue) and H₂ (black) produced in photocatalytic reduction of CO₂ in a mixture solution of DMA/H₂O (9:1, v/v; 4.0 mL) containing Mes-IrPCY2 (20 μM) and BIH (0.2 M) upon photoirradiation ($\lambda \geq 400$ nm) (a) under Ar atmosphere and (b) under CO₂ atmosphere without Mes-IrPCY2.

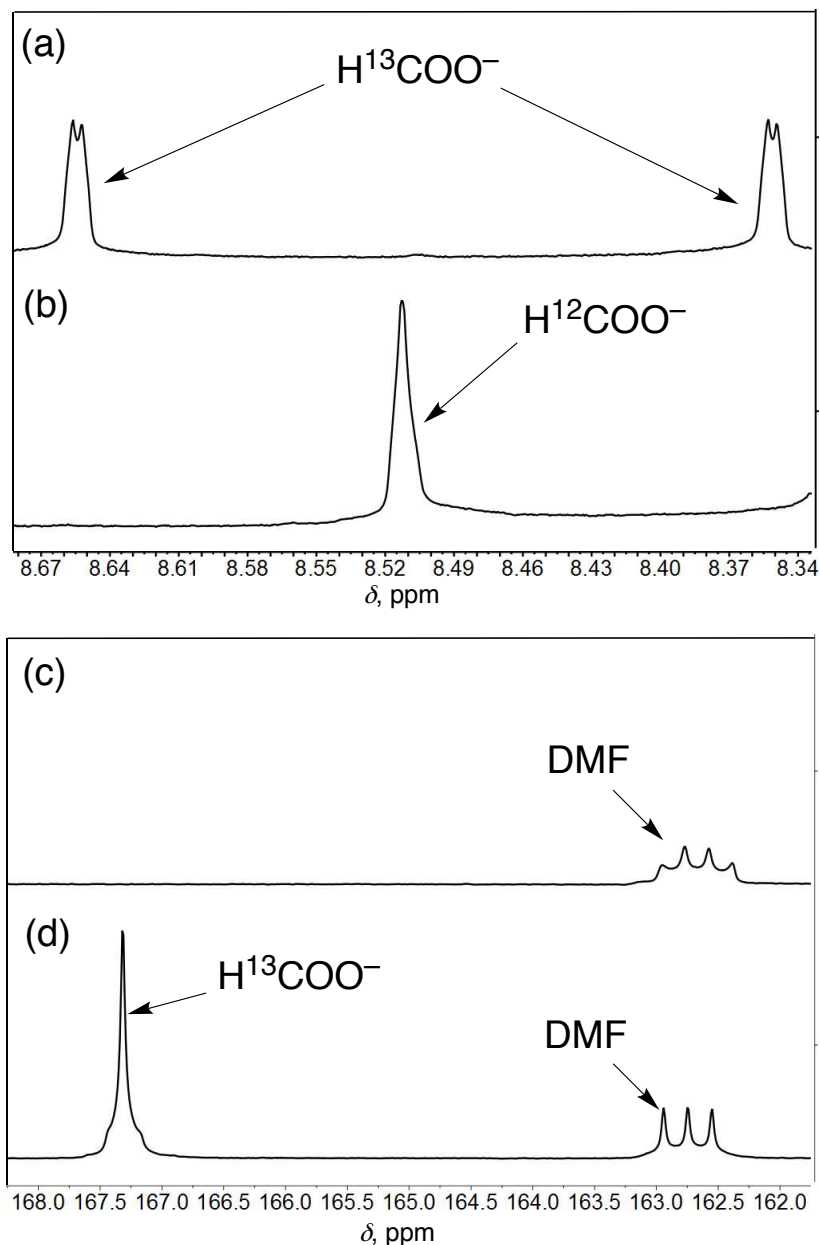


Figure S2. ^1H NMR spectra of the reaction solution after 24 h of photoirradiation ($\lambda \geq 400$ nm) on a mixture of $\text{DMF-}d_7/\text{H}_2\text{O}$ (9:1, v/v) containing Mes-IrPCY2 (0.1 mM) and BIH (0.1 M) under (a) $^{13}\text{CO}_2$ and (b) unlabeled CO_2 . A doublet attributable to the proton bound to the ^{13}C atom in H^{13}COOH was observed (Figure S2a) whereas a singlet was observed when an unlabeled CO_2 -saturated $\text{DMF-}d_7/\text{H}_2\text{O}$ (9:1, v/v) solution was used (Figure S2b). Proton-decoupled ^{13}C NMR spectrum of the photocatalytic reaction solution under $^{13}\text{CO}_2$ (c) before photoirradiation and (d) after 24 h of photoirradiation. These figures indicated that HCOOH was produced through the photocatalytic reduction of CO_2 .^{S8}

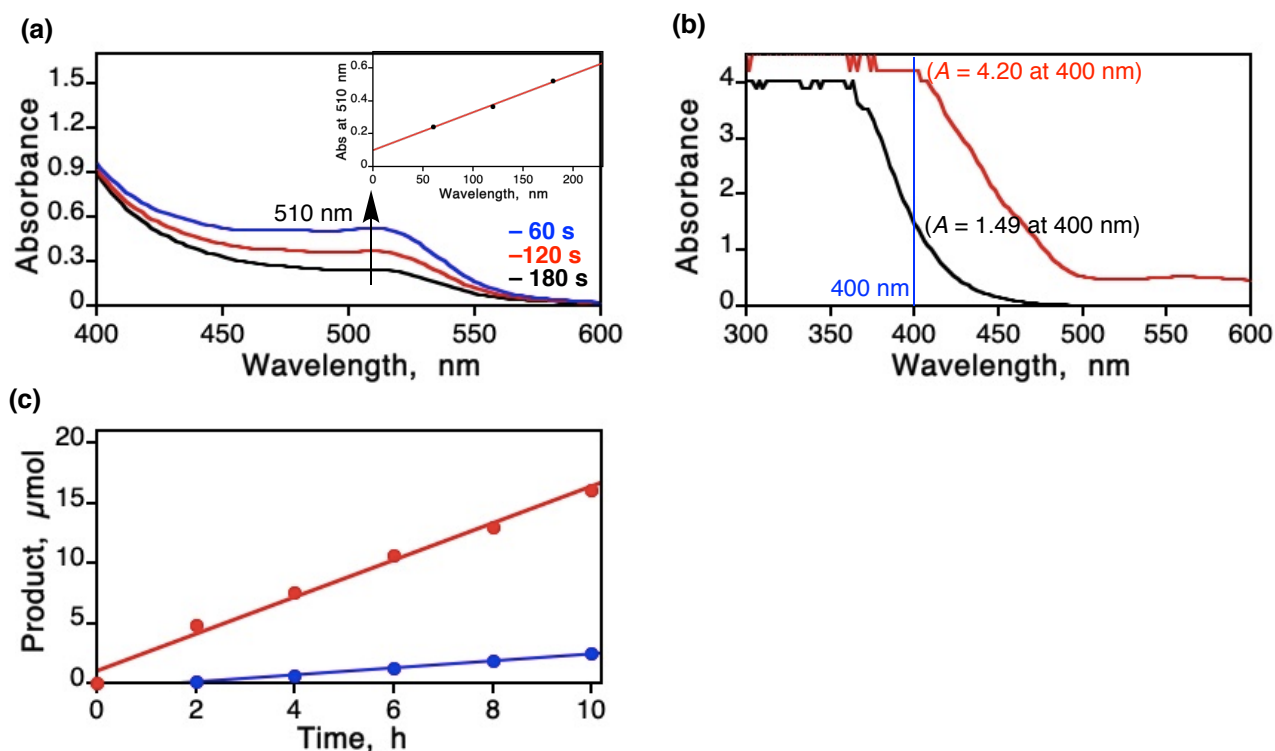


Figure S3. (a) UV-vis absorption spectral change of $[\text{Fe}(\text{phen})_3]^{2+}$ formed by the reaction of phenanthroline with Fe^{2+} ion, which was produced by photoirradiation of ferrioxalate actinometer using monochromatized light ($\lambda = 400$ nm) for 1, 2 and 3 min at 298 K. (b) UV-vis absorption spectral change of ferrioxalate actinometer [6.0 mM, Abs = 1.49, percentage of light absorption = $(1 - 10^{-1.49}) \times 100 = 96.8\%$; black line] using monochromatized light ($\lambda = 400$ nm) for 3 min and the reaction solution [Abs = 4.20, percentage of light absorption = $(1 - 10^{-4.20}) \times 100 = 100\%$; red line] obtained in the photocatalytic CO_2 reduction by Mes-IrPCY2 (1.5 mM) in presence of BIH (0.2 M) under photoirradiation for 5 h with monochromatized light ($\lambda = 400$ nm) in CO_2 -saturated mixture of DMA/ H_2O (9:1, v/v; 4.0 mL) at 298 K. (c) Time courses of formation of HCOOH (red) and CO (blue) produced in the photocatalytic reduction of CO_2 in the presence of BIH (0.2 M) in a CO_2 -saturated mixture of DMA/ H_2O (9:1, v/v; 4.0 mL) containing Mes-IrPCY2 (1.5 mM) under photoirradiation with monochromatized light ($\lambda = 400$ nm) for 10 h.

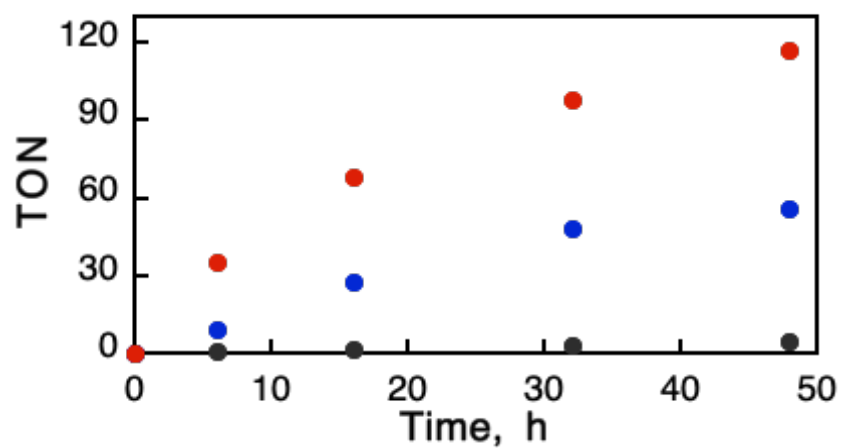


Figure S4. Time courses of products [HCOOH (red), CO (blue), and H₂ (black)] obtained in the photocatalytic CO₂ reduction with Mes-IrPCY2 (20 μM) in a CO₂-saturated mixture of DMA/H₂O/TEOA (9:1:2, v/v/v) under photoirradiation ($\lambda \geq 400$ nm) at 298 K.

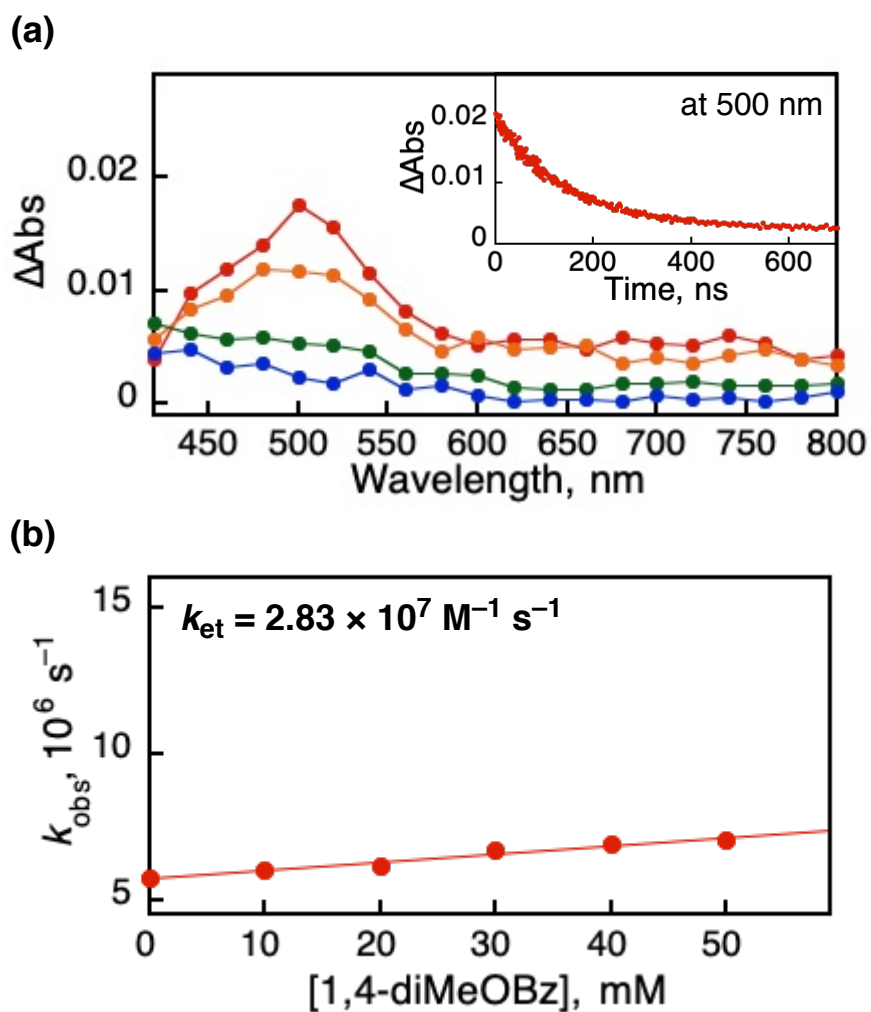


Figure S5. (a) Transient absorption spectral changes (red 2 ns, orange 50 ns, green 200 ns, and blue 500 ns) after sub-nanosecond laser excitation at 355 nm in deaerated DMA containing Mes-IrPCY2 (1.0 mM) and 1,4-dimethoxybenzene (1,4-diMeOBz, 100 mM) at 298 K. Inset shows the decay time profile of the absorbance at 500 nm due to the decay of the excited state of Mes-IrPCY2. (b) Plot of k_{obs} vs concentration of 1,4-dimethoxybenzene (0 – 100 mM) in DMA at 298 K.

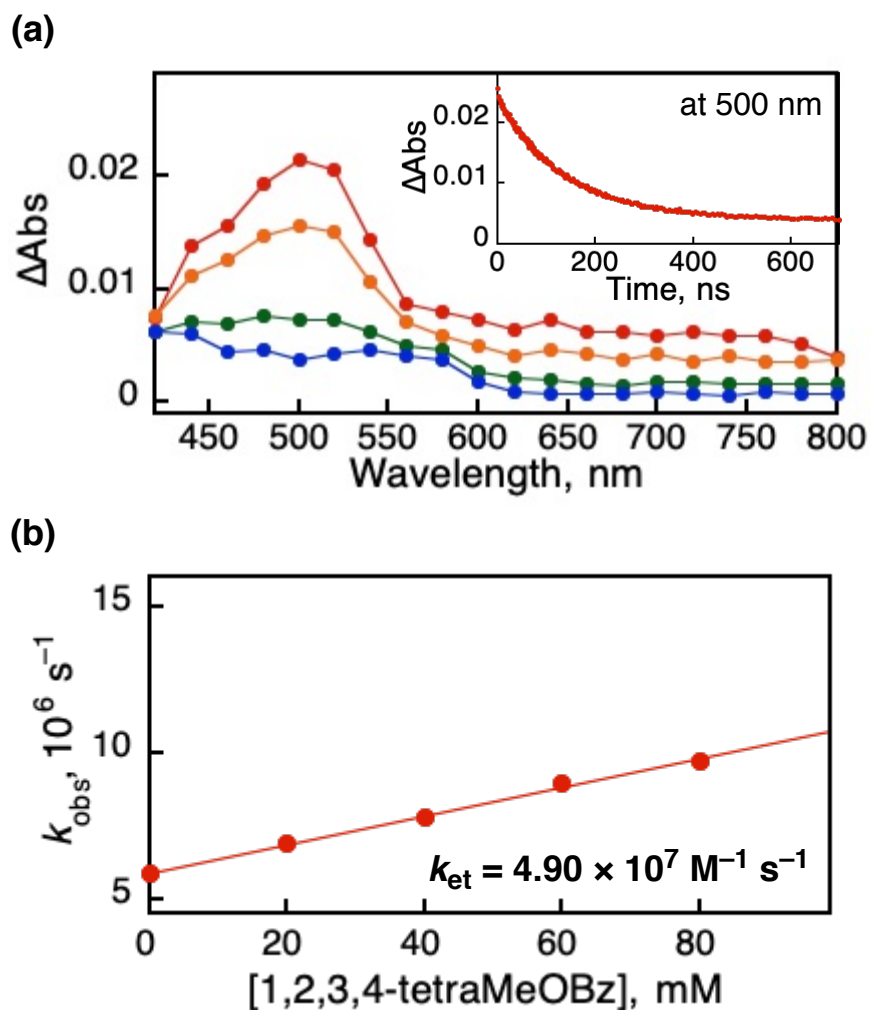


Figure S6. (a) Transient absorption spectral changes (red 2 ns, orange 50 ns, green 200 ns, and blue 500 ns) after sub-nanosecond laser excitation at 355 nm in deaerated DMA containing Mes-IrPCY2 (1.0 mM) and 1,2,3,4-tetramethoxybenzene (1,2,3,4-tetraMeOBe, 50 mM) at 298 K. Inset shows the decay time profile of the absorbance at 500 nm due to the decay of the excited state of Mes-IrPCY2. (b) Plot of k_{obs} vs concentration of 1,2,3,4-tetramethoxybenzene (0 – 50 mM) in DMA at 298 K.

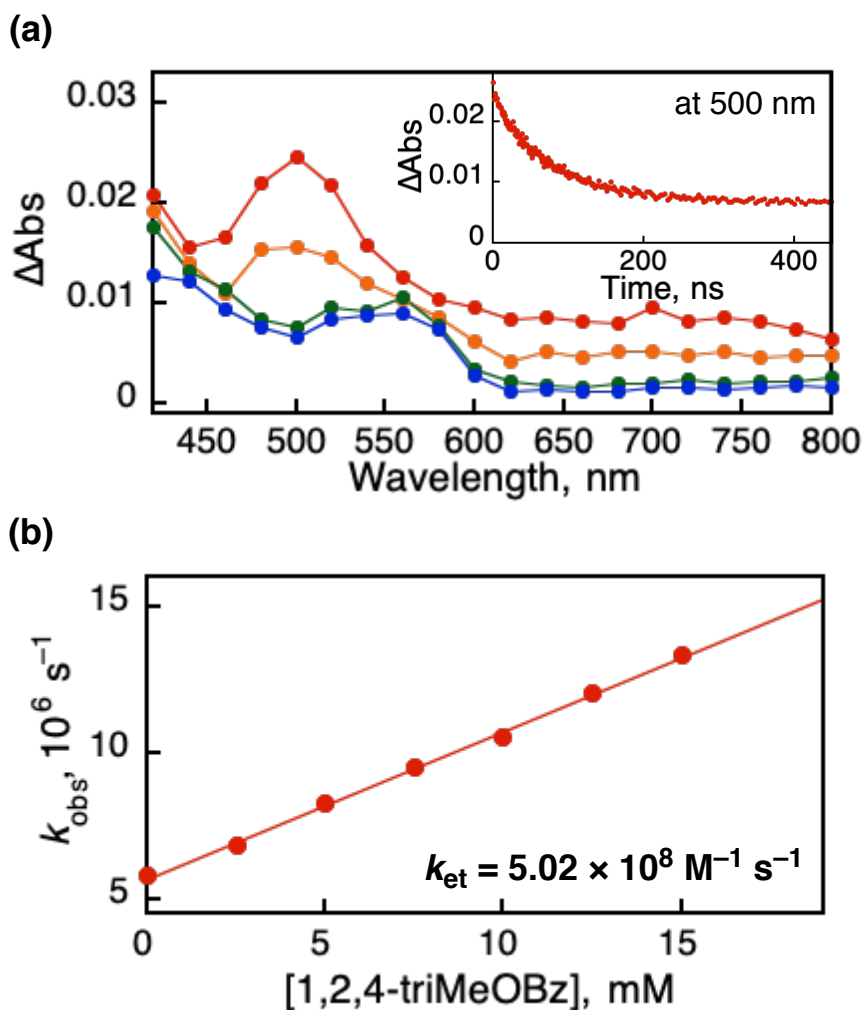


Figure S7. (a) Transient absorption spectral changes (red 2 ns, orange 50 ns, green 200 ns, and blue 500 ns) after sub-nanosecond laser excitation at 355 nm in deaerated DMA containing Mes-IrPCY2 (1.0 mM) and 1,2,4-trimethoxybenzene (1,2,4-triMeOBz, 15 mM) at 298 K. Inset shows the decay time profile of the absorbance at 500 nm due to the decay of the excited state of Mes-IrPCY2. (b) Plot of k_{obs} vs concentration of 1,2,4-trimethoxybenzene (0 – 15 mM) in DMA at 298 K.

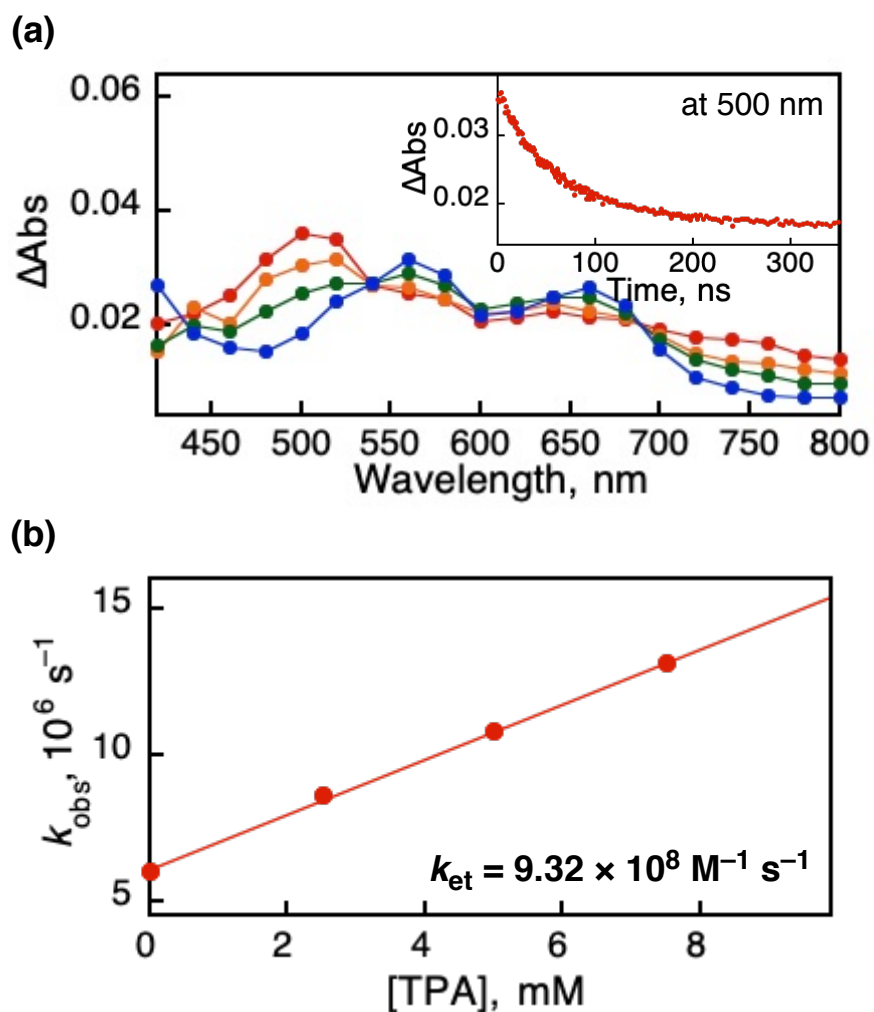


Figure S8. (a) Transient absorption spectral changes (red 2 ns, orange 20 ns, green 50 ns, and blue 200 ns) after sub-nanosecond laser excitation at 355 nm in deaerated DMA containing Mes-IrPCY2 (1.0 mM) and triphenylamine (TPA, 7.5 mM) at 298 K. Inset shows the decay time profile of the absorbance at 500 nm due to the decay of the excited state of Mes-IrPCY2. (b) Plot of k_{obs} vs concentration of triphenylamine (0 – 7.5 mM) in DMA at 298 K.

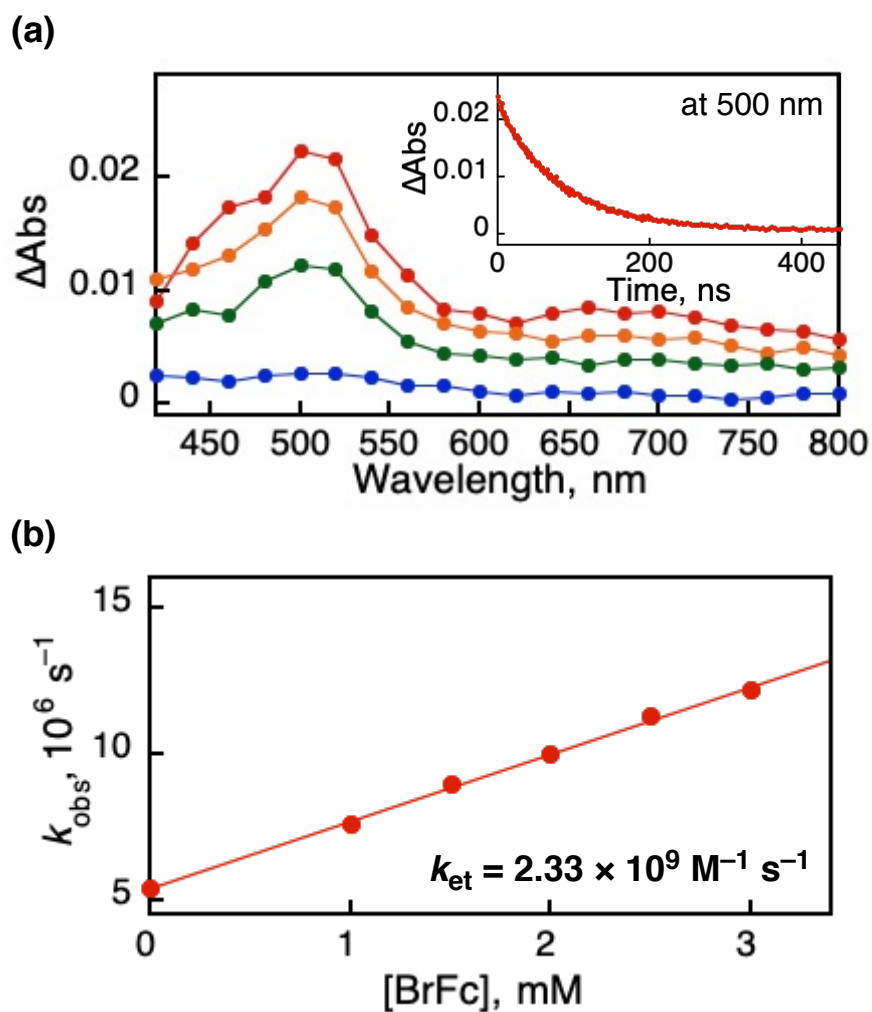


Figure S9. (a) Transient absorption spectral changes (red 2 ns, orange 20 ns, green 50 ns, and blue 200 ns) after sub-nanosecond laser excitation at 355 nm in deaerated DMA containing Mes-IrPCY2 (1.0 mM) and bromoferrocene (BrFc, 3.0 mM) at 298 K. Inset shows the decay time profile of the absorbance at 500 nm due to the decay of the excited state of Mes-IrPCY2. (b) Plot of k_{obs} vs concentration of bromoferrocene (0 – 3.0 mM) in DMA at 298 K.

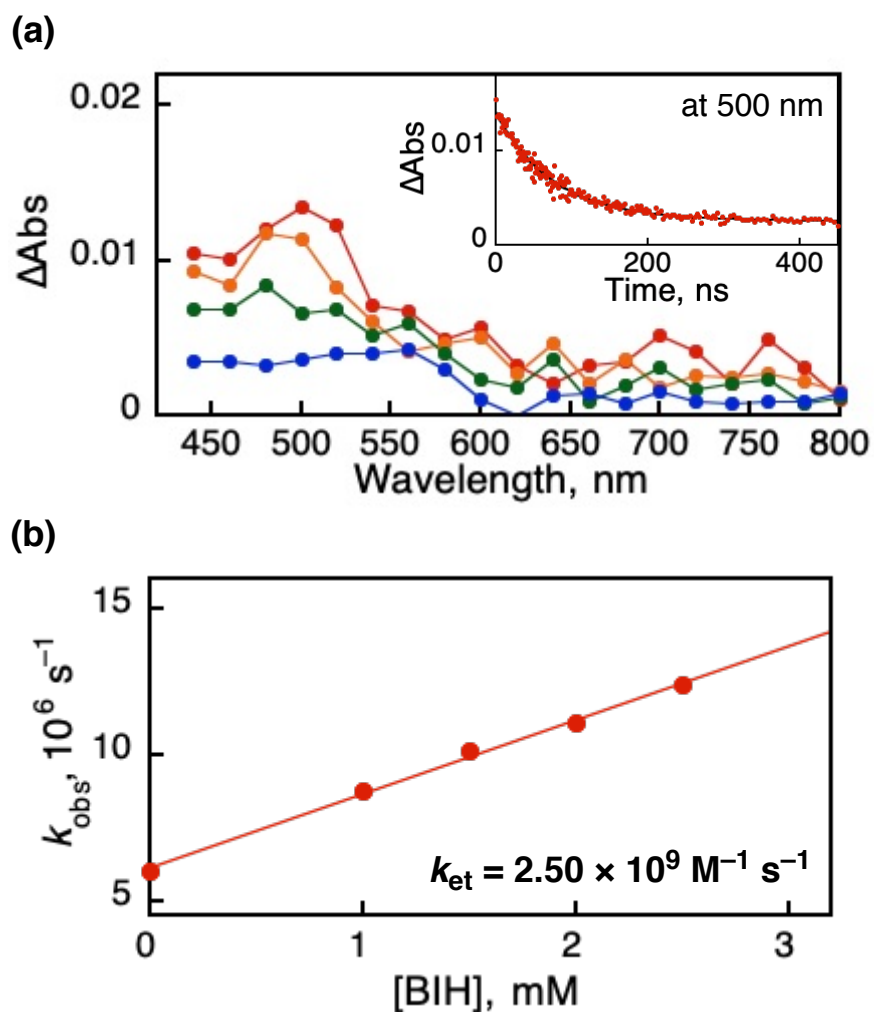


Figure S10. (a) Transient absorption spectral changes (red 2 ns, orange 20 ns, green 50 ns, and blue 200 ns) after sub-nanosecond laser excitation at 355 nm in deaerated DMA containing Mes-IrPCY2 (1.0 mM) and BIH (2.5 mM) at 298 K. Inset shows the decay time profile of the absorbance at 500 nm due to the decay of the excited state of Mes-IrPCY2. (b) Plot of k_{obs} vs concentration of BIH (0 – 2.5 mM) in DMA at 298 K.

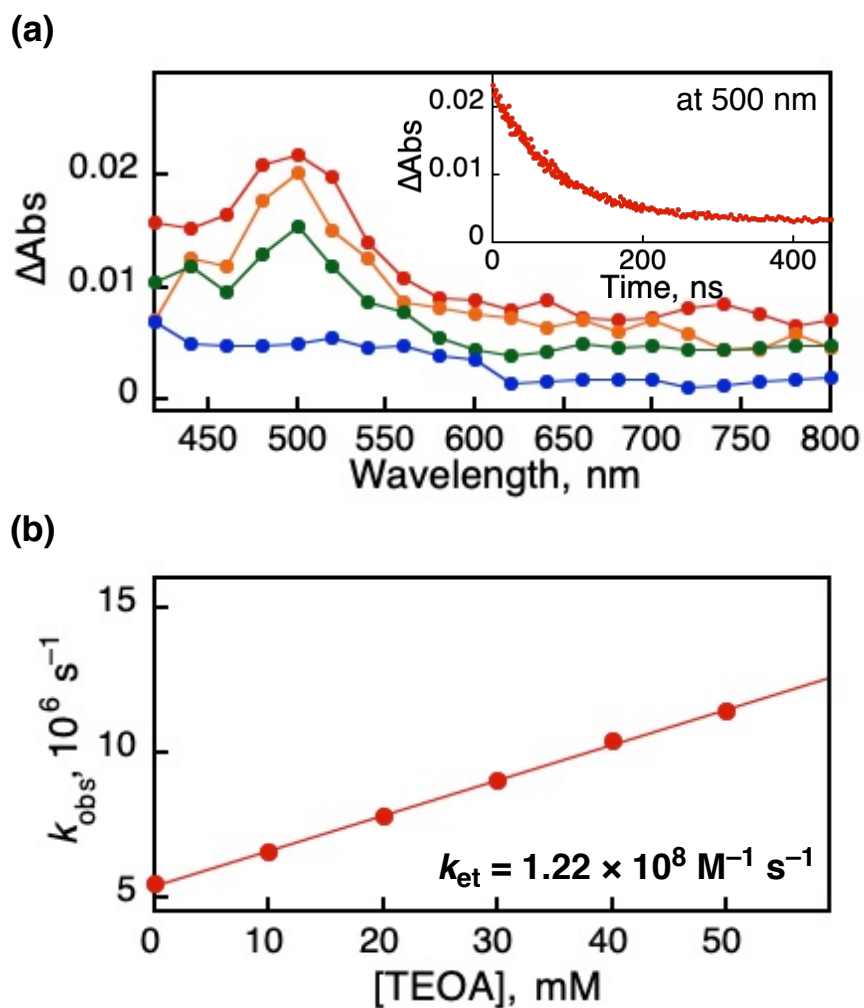


Figure S11. (a) Transient absorption spectral changes (red 2 ns, orange 20 ns, green 50 ns, and blue 200 ns) after sub-nanosecond laser excitation at 355 nm in deaerated DMA containing Mes-IrPCY2 (1.0 mM) and TEOA (50 mM) at 298 K. Inset shows the decay time profile of the absorbance at 500 nm due to the decay of the excited state of Mes-IrPCY2. (b) Plot of k_{obs} vs concentration of TEOA (0 – 50 mM) in DMA at 298 K.

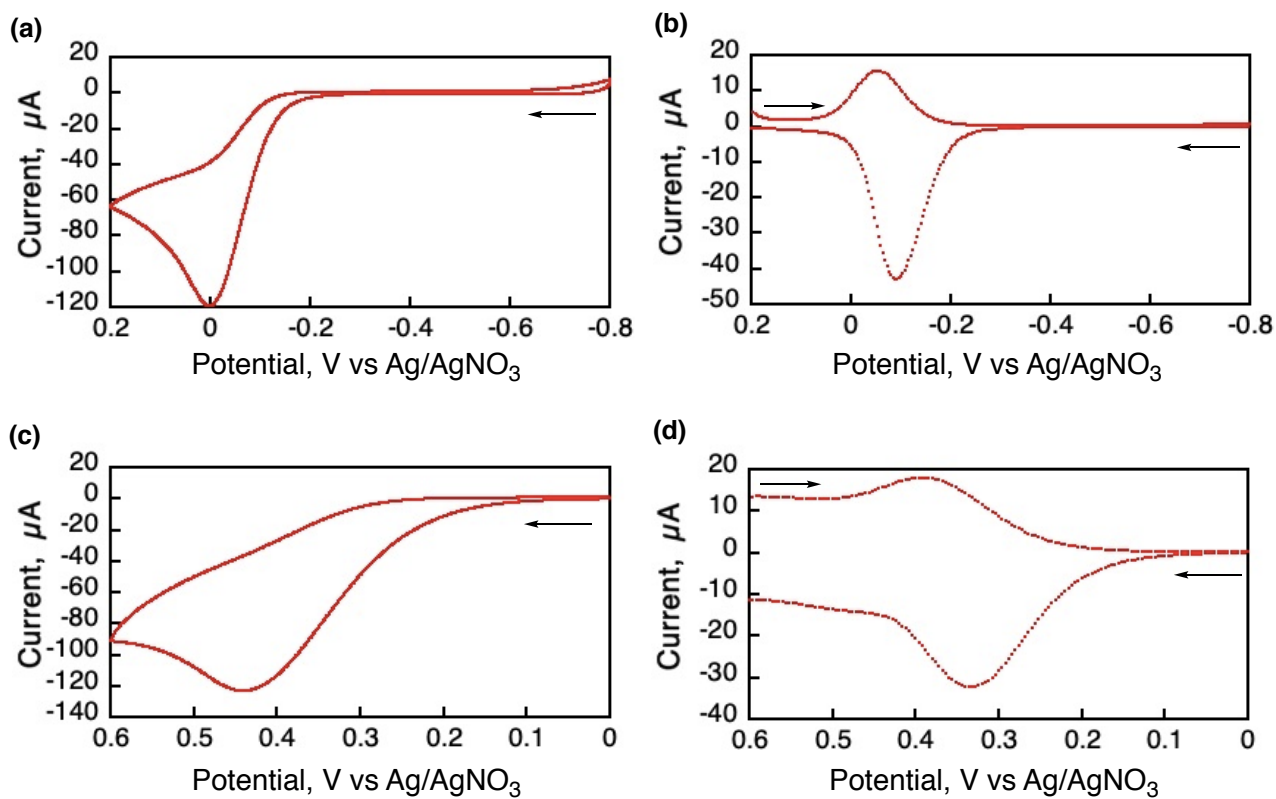


Figure S12. (a) CV and (b) DPV of BIH (5.0 mM); (c) CV and (d) DPV of TEOA (5.0 mM) under Ar atmospheres. For all measurements, 0.10 M NEt₄BF₄ was used as a supporting electrode and Ag/AgNO₃ (10 mM) was used as a reference electrode; scan rate of CV: 100 mV/s.

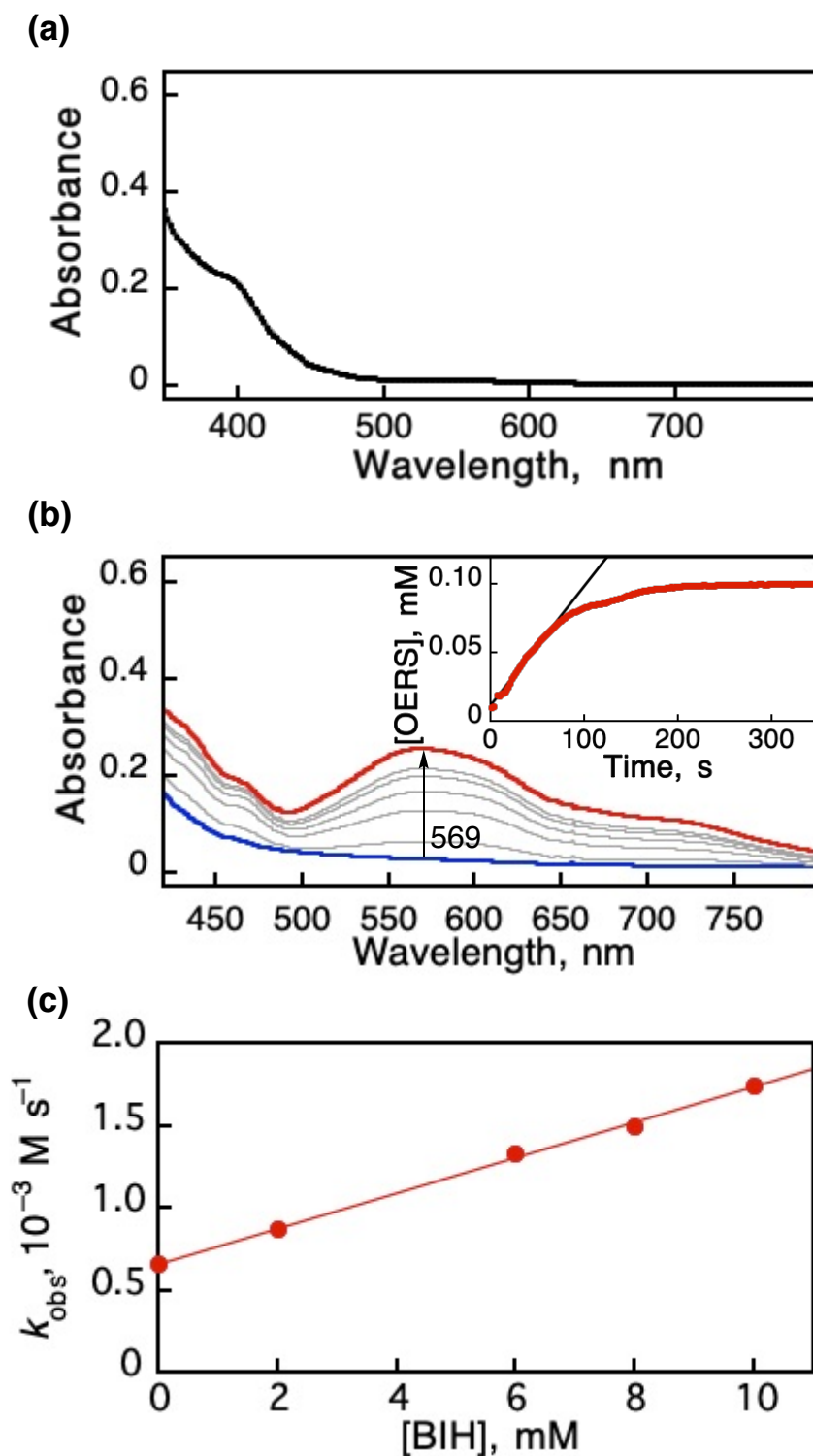


Figure S13. (a) UV-Vis absorption spectrum of Mes-IrPCY2 (0.1 mM) in DMA/H₂O (9:1, v/v) under Ar at 298 K. (b) UV-Vis spectral change of Mes-IrPCY2 in the presence of BIH upon photoirradiation ($\lambda \geq 400$ nm) on an Ar-saturated mixture of DMA/H₂O (9:1, v/v) containing Mes-IrPCY2 (0.1 mM) in the presence of BIH (2.0 mM) at 298 K. (c) Plot of the initial rate (k_{obs}) vs concentration of BIH.

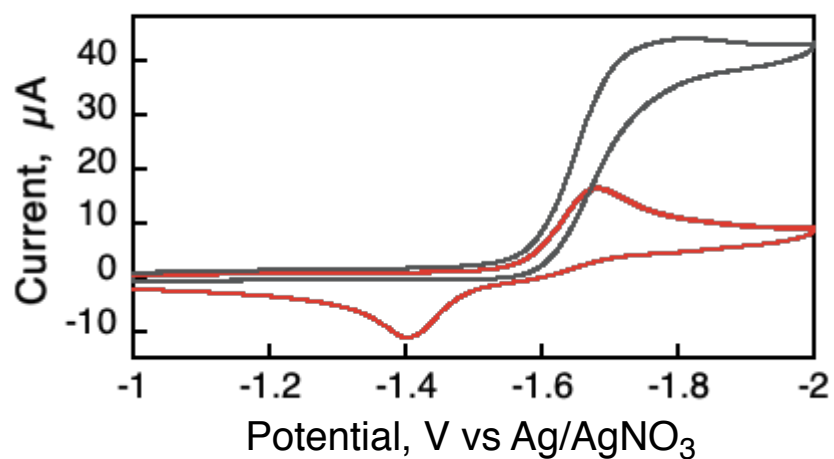


Figure S14. Cyclic voltammetry of Mes-IrPCY2 (1.0 mM) in DMA solution containing 0.1 M Et_4NBF_4 as a supporting electrolyte and Ag/AgNO_3 (10 mM) as a reference electrode under Ar atmosphere (red) and CO_2 atmosphere (gray). Scan rate: 0.1 V s^{-1} .

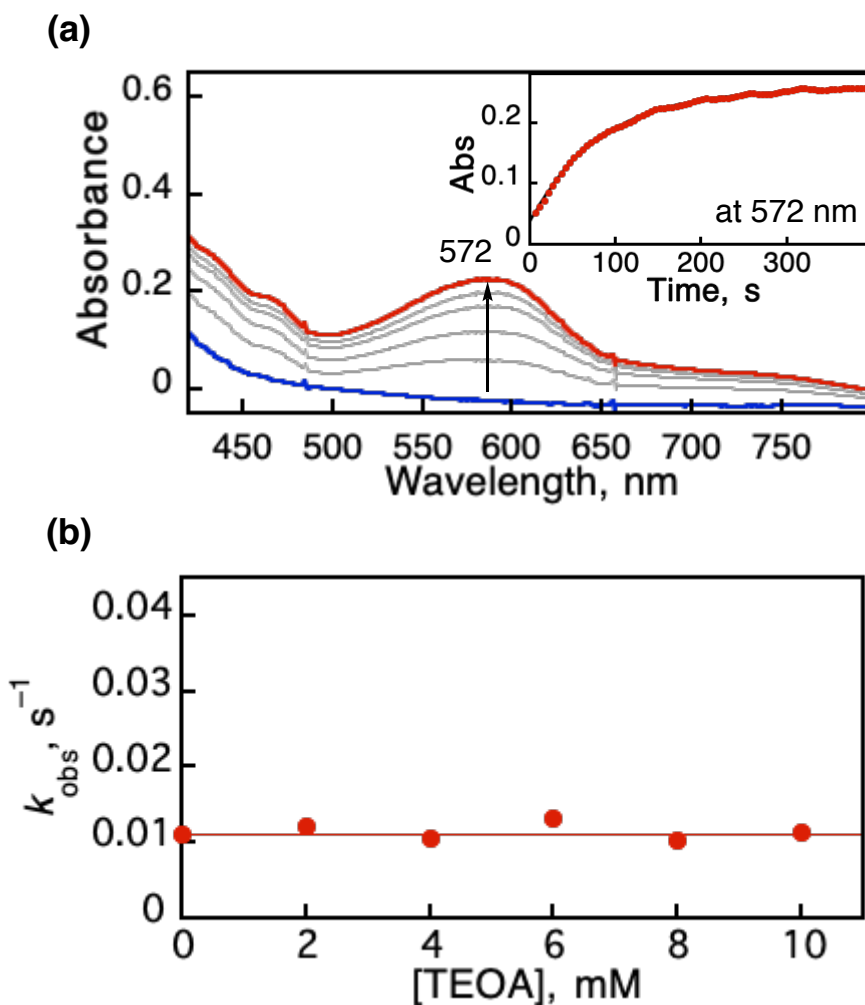


Figure S15. (a) UV-Vis spectral change of Mes-IrPCY2 in the presence of TEOA upon photoirradiation ($\lambda \geq 400$ nm) on an Ar-saturated mixture of DMA/H₂O (9:1, v/v) containing Mes-IrPCY2 (0.1 mM) in the presence of TEOA (0 – 10 mM) at 298 K. (b) Plot of the formation of Ir^I (k_{obs}) vs concentration of TEOA. In competition with formation of OERS, the amounts of TEOA (< 10 mM) are not enough to mainly form OERS in these kinetic experiments compared with those for CO₂ photo-reduction (*ca.* 1.3 M in Figure S4), leading to deprotonation of Ir(III)–H predominantly.

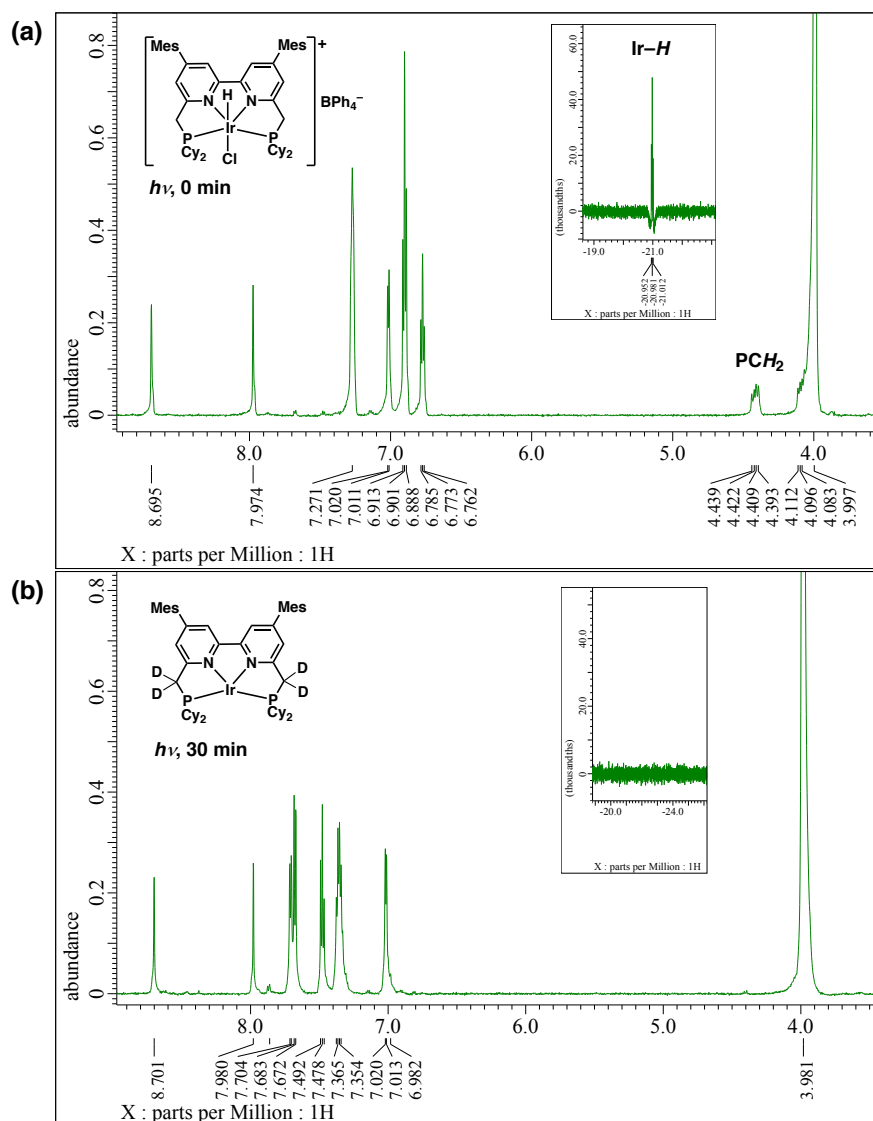
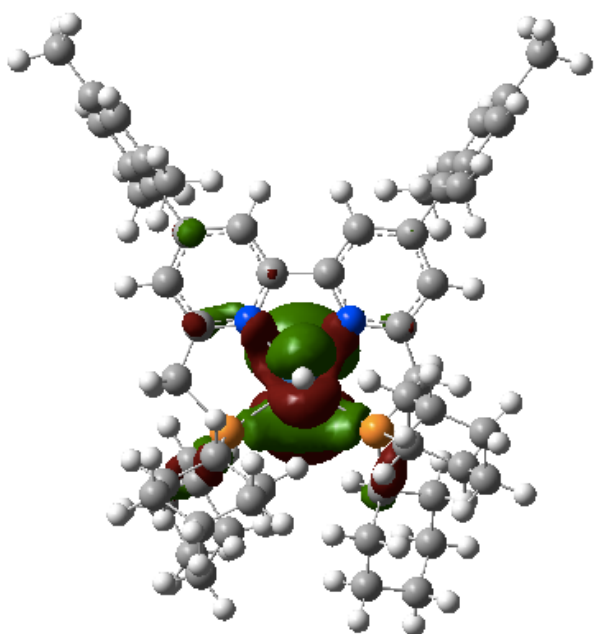


Figure S16. ^1H NMR spectra of a mixture of $\text{DMA-}d_9/\text{D}_2\text{O}$ (9:1, v/v) containing Mes-IrPCY2 (4 mM) under CO_2 (a) before photoirradiation and (b) after 30 min of photoirradiation ($\lambda \geq 400$ nm). Although it's difficult to distinguish whether Ir(I) or Ir(III)-D complex was formed after photoirradiation from the NMR spectra, a distinct new absorption at 572 nm in UV-vis spectral change (Figure S15) suggest that Ir(I) complex is formed rather than incorporation of D under photoirradiation.

(a) HOMO



(b) LUMO

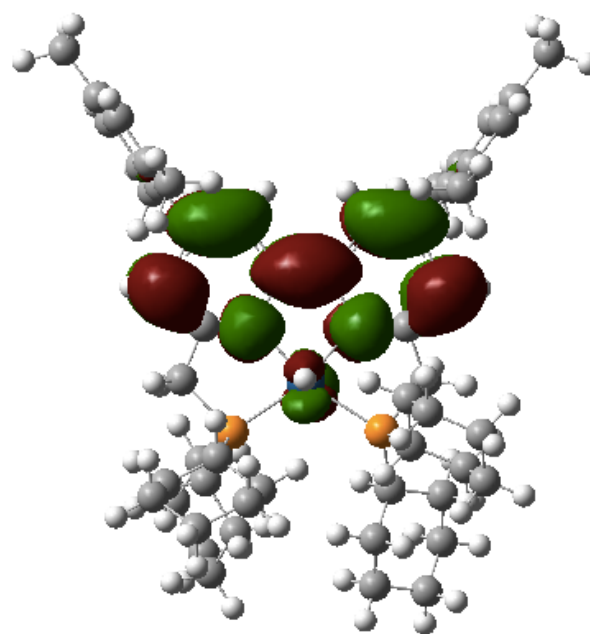


Figure S17. DFT calculation of Mes-IrPCY2. (a) HOMO; (b) LUMO images. The molecular structure and the energy were obtained at the B3LYP level with LANL2DZ with f-type pseudopotentials for Ir and 6-31G** for the other atoms. Since HOMO is located on iridium atom and LUMO is mainly on bipyridine moiety, metal-to-ligand charge-transfer occurs by photoirradiation. Because the basicity of iridium center is decreased in such the excited state, proton would be released easily from the Ir complex by light irradiation.

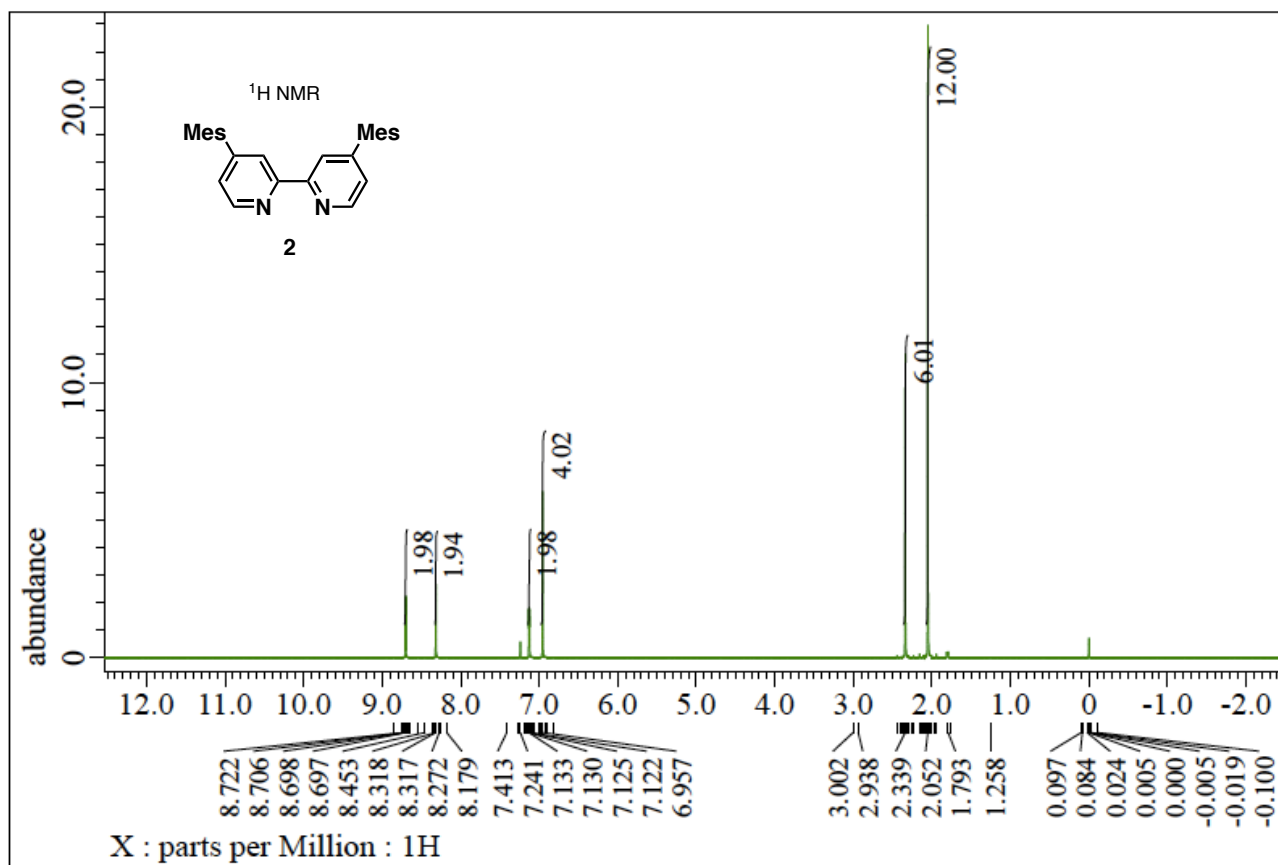


Figure S18. ¹H NMR spectrum of 4,4'-bis(2,4,6-trimethylphenyl)-2,2'-bipyridine (2).

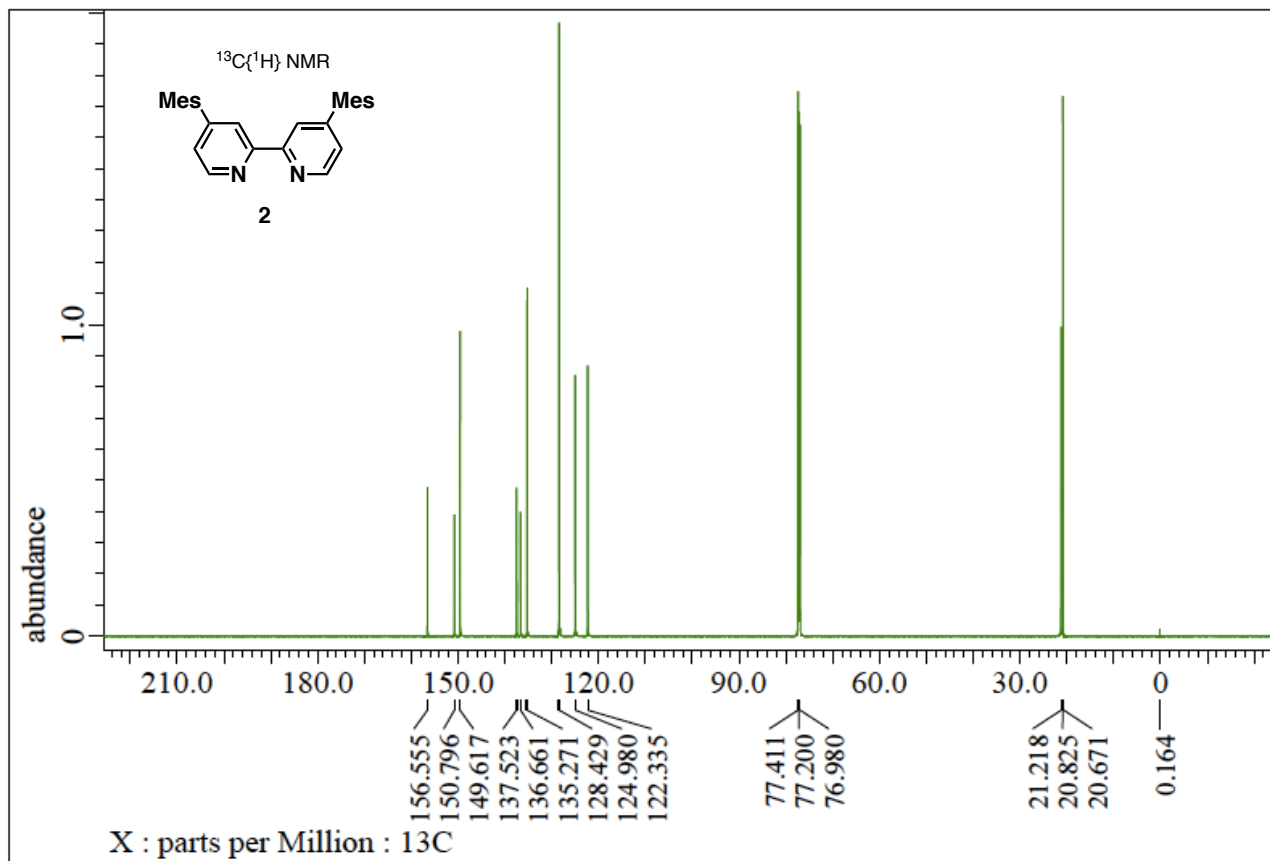


Figure S19. ¹³C{¹H} NMR spectrum of 4,4'-bis(2,4,6-trimethylphenyl)-2,2'-bipyridine (**2**).

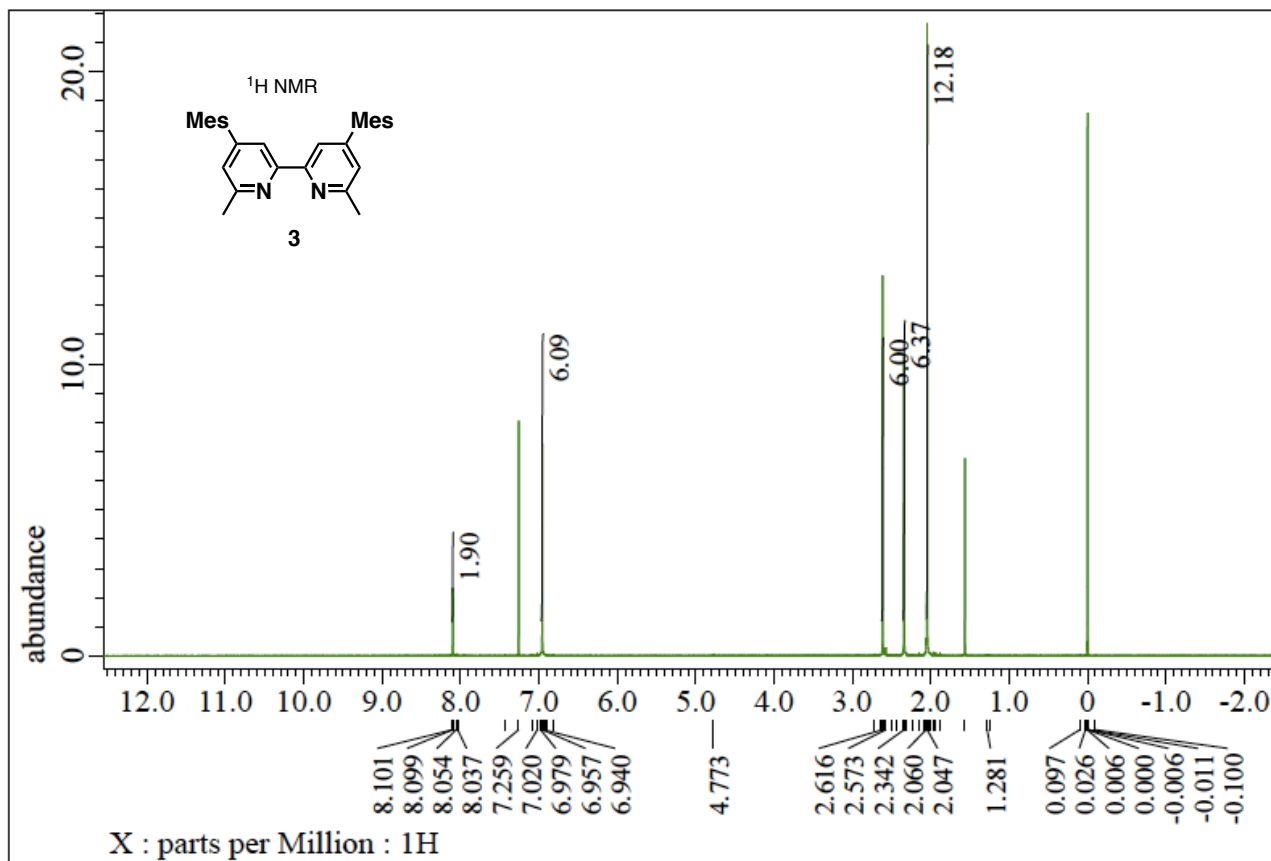


Figure S20. ¹H NMR spectrum of 4,4'-bis(2,4,6-trimethylphenyl)-6,6'-dimethyl-2,2'-bipyridine (3).

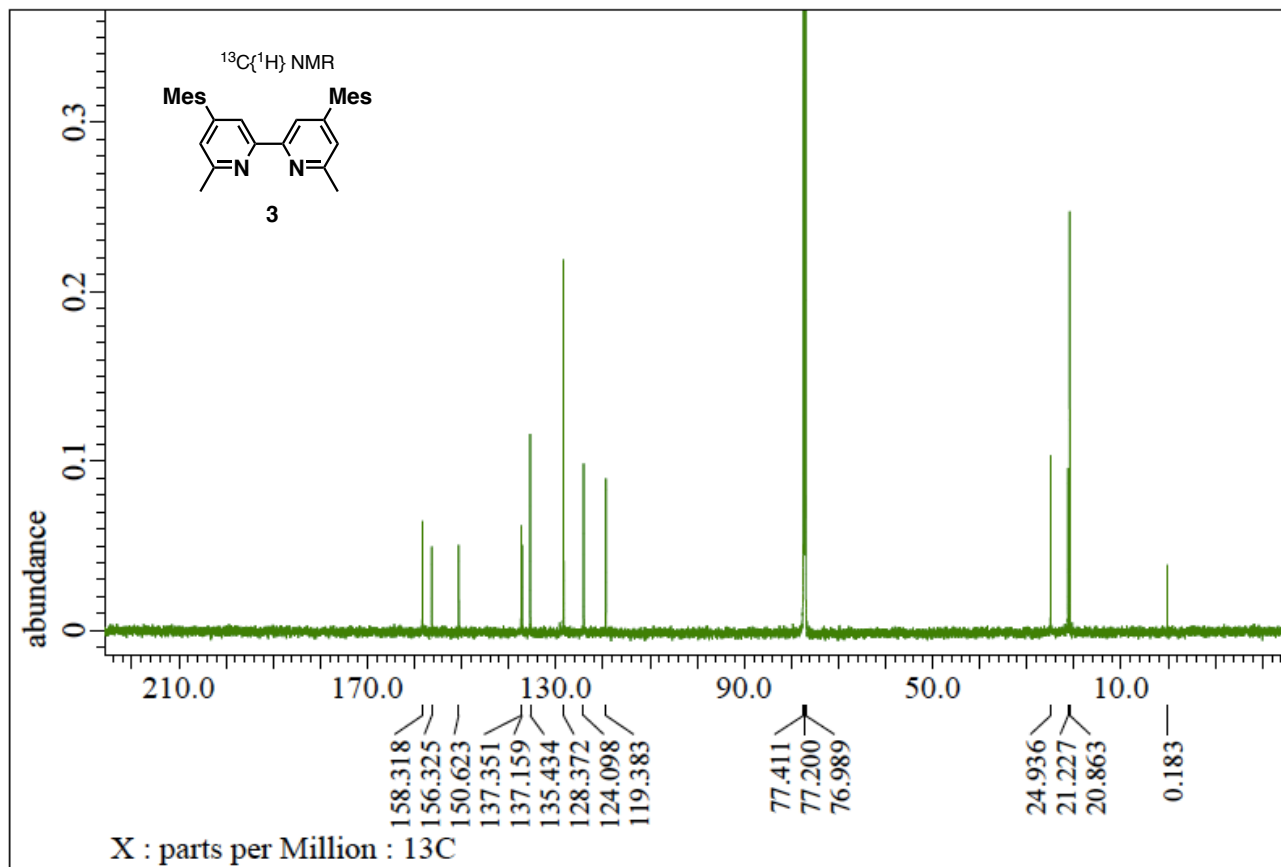


Figure S21. ¹³C{¹H} NMR spectrum of 4,4'-bis(2,4,6-trimethylphenyl)-6,6'-dimethyl-2,2'-bipyridine (**3**).

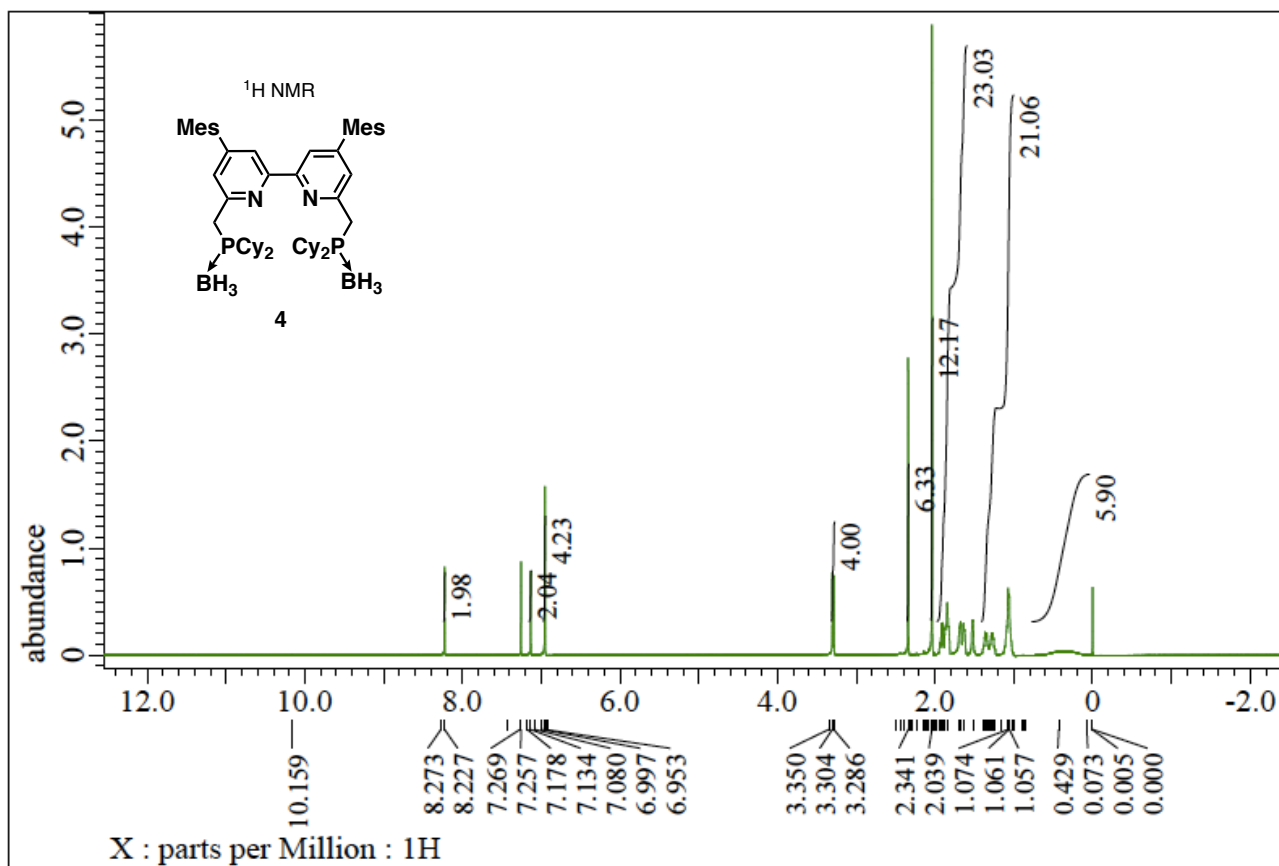


Figure S22. ¹H NMR spectrum of 6,6'-bis((dicyclohexylphosphino)methyl)-4,4'-bis(2,4,6-trimethylphenyl)-2,2'-bipyridine-diborane complex (4).

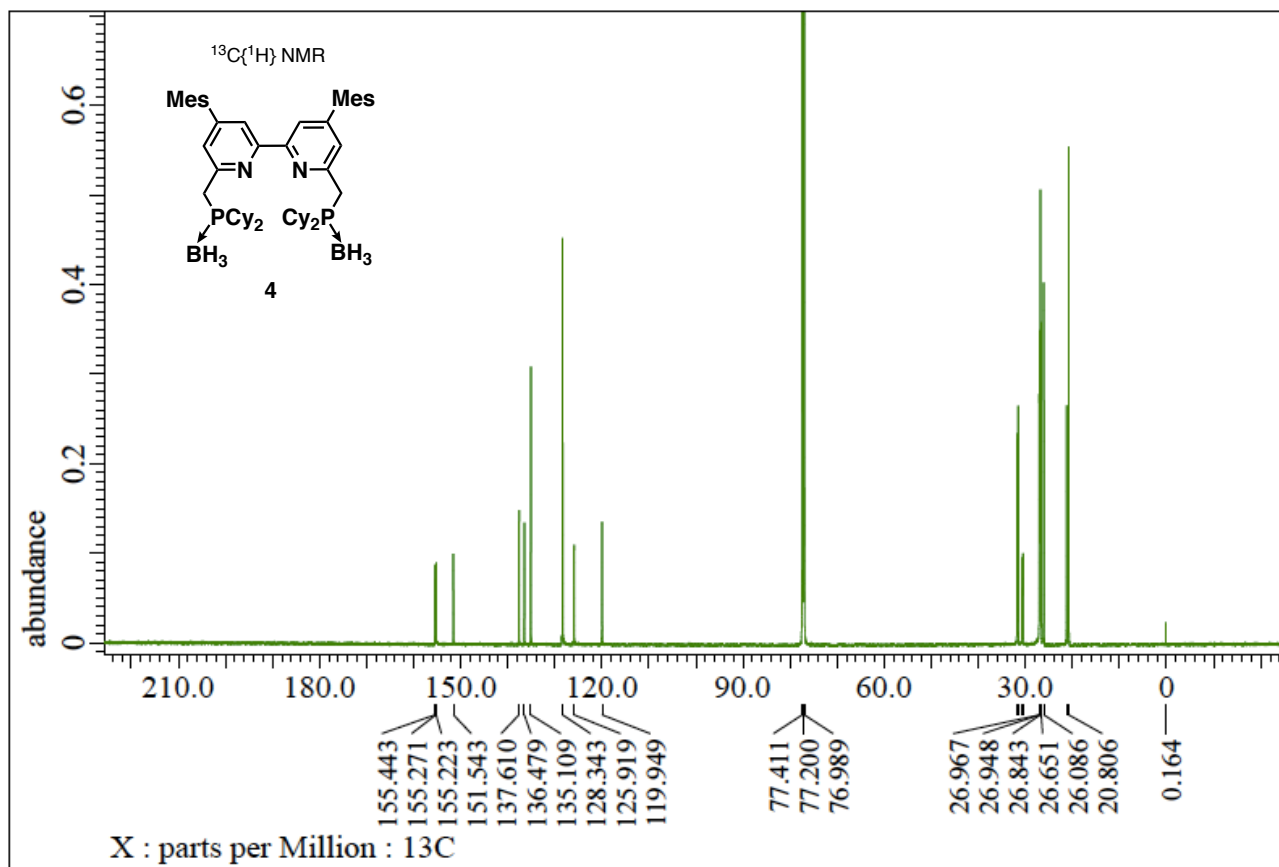


Figure S23. ¹³C{¹H} NMR spectrum of 6,6'-bis((dicyclohexylphosphino)methyl)-4,4'-bis(2,4,6-trimethylphenyl)-2,2'-bipyridine-diborane complex (4).

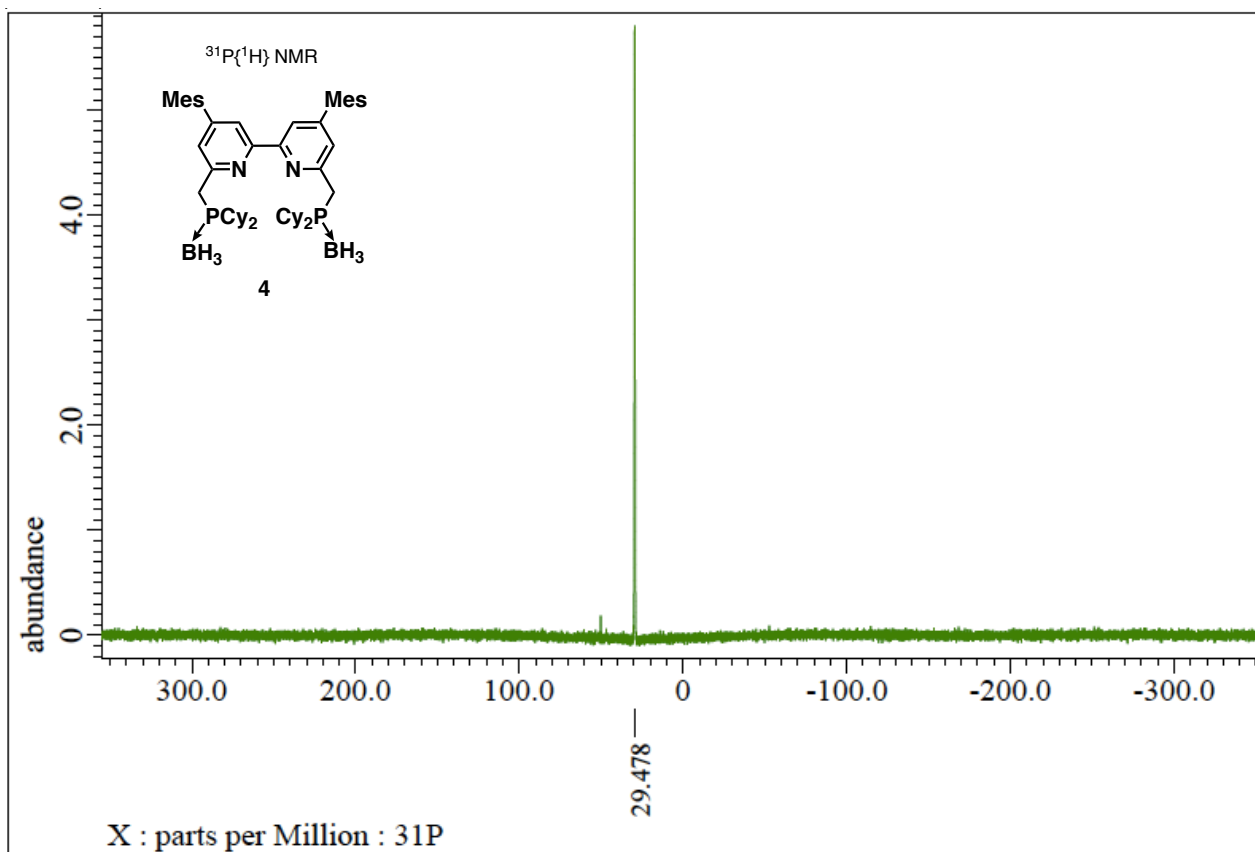


Figure S24. $^{31}\text{P}\{^1\text{H}\}$ NMR spectrum of 6,6'-bis((dicyclohexylphosphino)methyl)-4,4'-bis(2,4,6-trimethylphenyl)-2,2'-bipyridine-diborane complex (4).

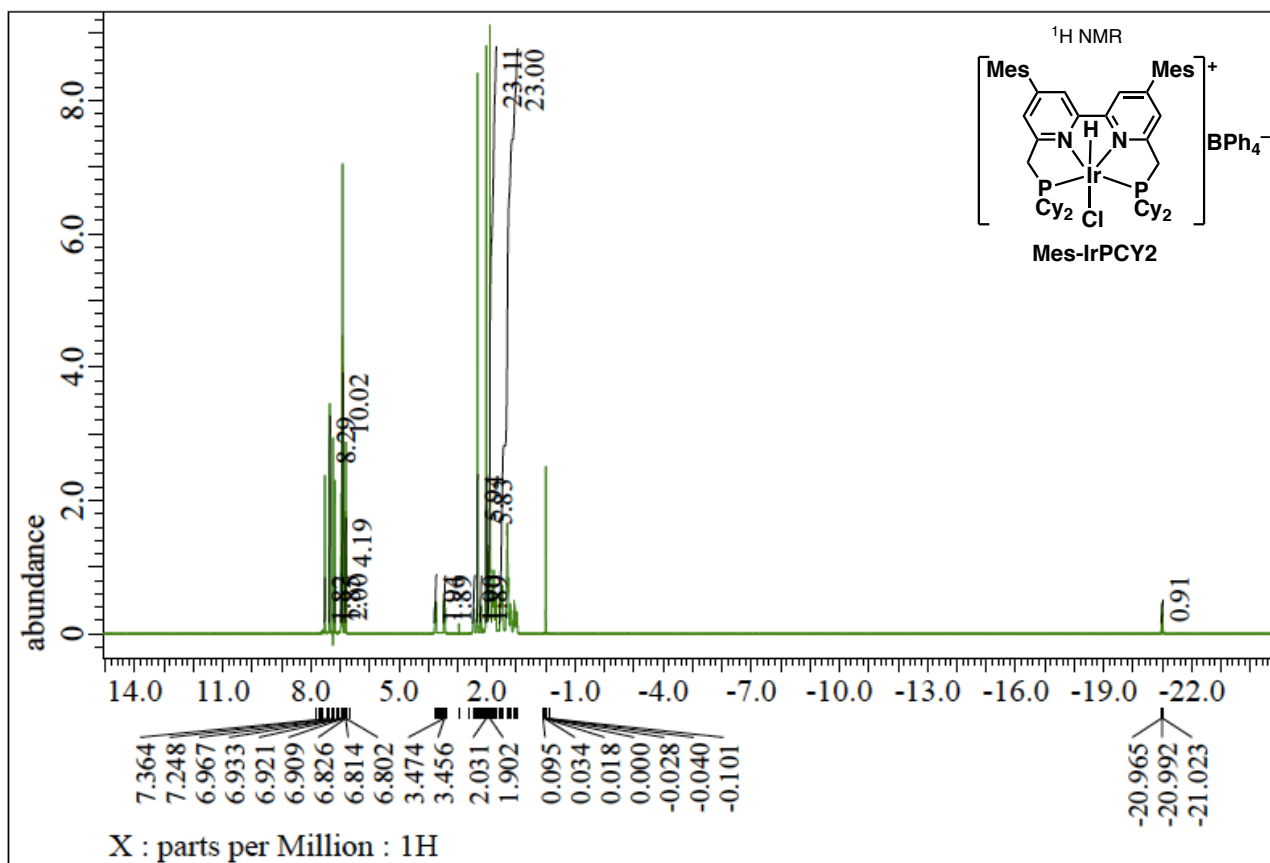


Figure S25. ^1H NMR spectrum of Mes-IrPCY2 (5).

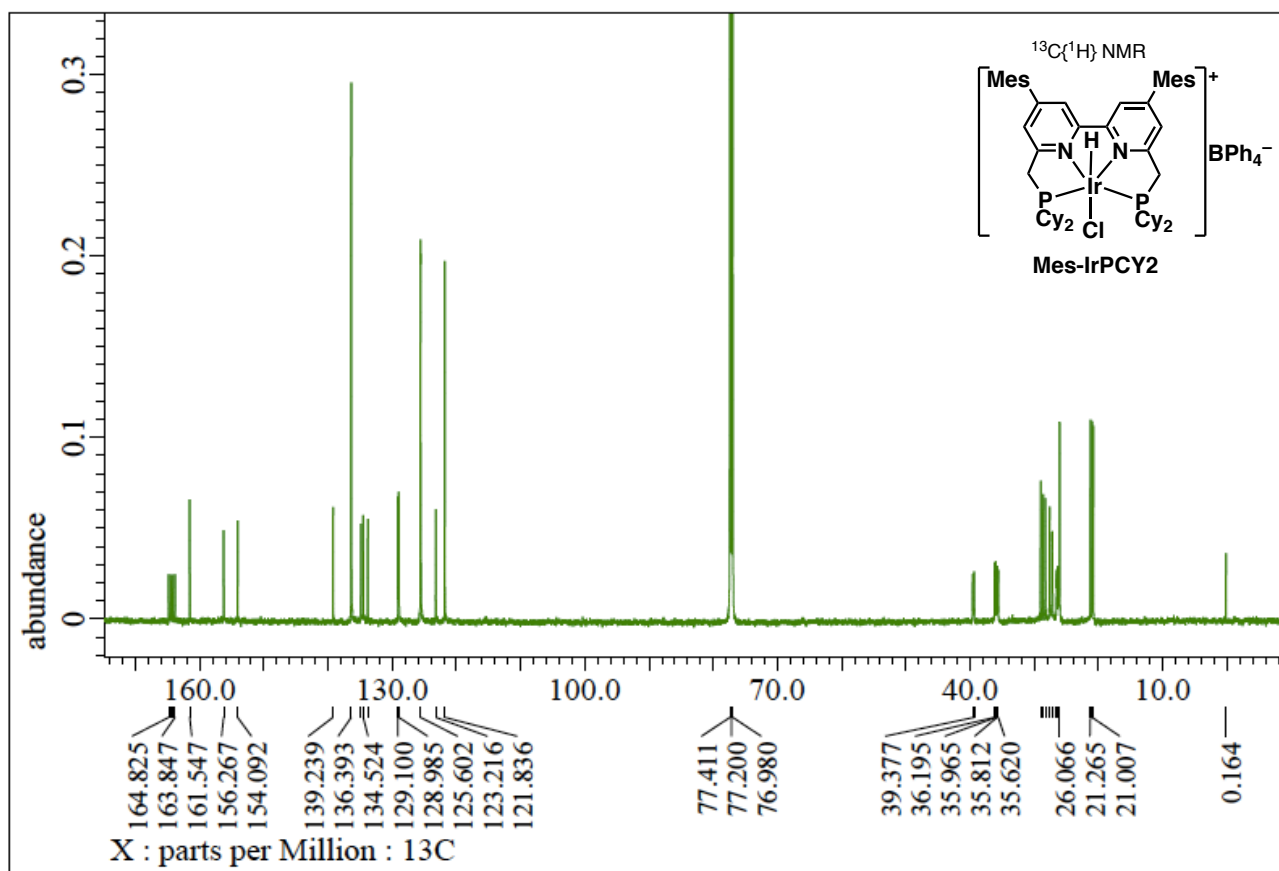


Figure S26. $^{13}\text{C}\{^1\text{H}\}$ NMR spectrum of Mes-IrPCY2 (5).

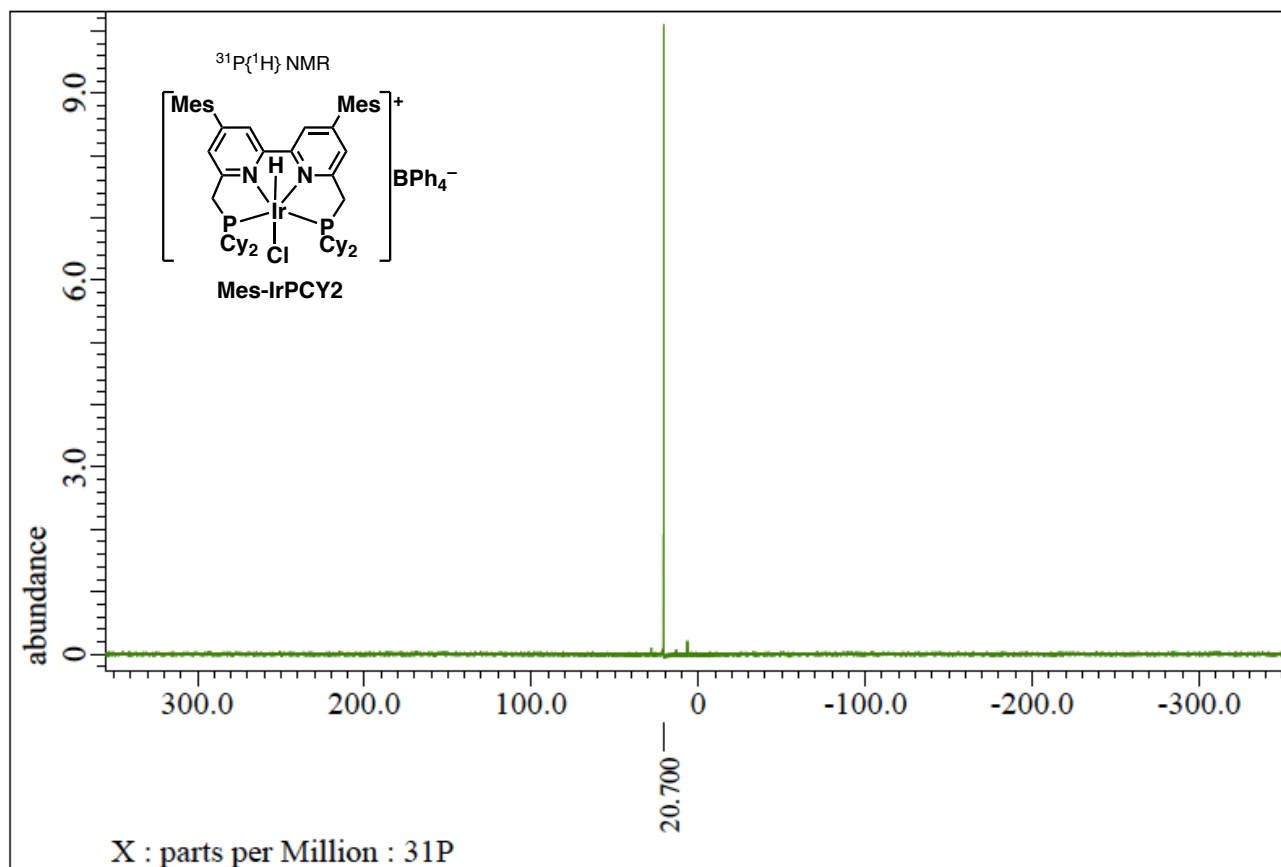


Figure S27. $^{31}\text{P}\{^1\text{H}\}$ NMR spectrum of Mes-IrPCY2 (5).

References

- (S1) Gaussian 09, Revision B.01, Frisch, M. J.; Trucks, G. W.; Schlegel, H. B.; Scuseria, G. E.; Robb, M. A.; Cheeseman, J. R.; Scalmani, G.; Barone, V.; Mennucci, B.; Petersson, G. A.; Nakatsuji, H.; Caricato, M.; Li, X.; Hratchian, H. P.; Izmaylov, A. F.; Bloino, J.; Zheng, G.; Sonnenberg, J. L.; Hada, M.; Ehara, M.; Toyota, K.; Fukuda, R.; Hasegawa, J.; Ishida, M.; Nakajima, T.; Honda, Y.; Kitao, O.; Nakai, H.; Vreven, T.; Montgomery, Jr., J. A.; Peralta, J. E.; Ogliaro, F.; Bearpark, M.; Heyd, J. J.; Brothers, E.; Kudin, K. N.; Staroverov, V. N.; Keith, T.; Kobayashi, R.; Normand, J.; Raghavachari, K.; Rendell, A.; Burant, J. C.; Iyengar, S. S.; Tomasi, J.; Cossi, M.; Rega, N.; Millam, J. M.; Klene, M.; Knox, J. E.; Cross, J. B.; Bakken, V.; Adamo, C.; Jaramillo, J.; Gomperts, R.; Stratmann, R. E.; Yazyev, O.; Austin, A. J.; Cammi, R.; Pomelli, C.; Ochterski, J. W.; Martin, R. L.; Morokuma, K.; Zakrzewski, V. G.; Voth, G. A.; Salvador, P.; Dannenberg, J. J.; Dapprich, S.; Daniels, A. D.; Farkas, O.; Foresman, J. B.; Ortiz, J. V.; Cioslowski, J.; Fox, D. J. Gaussian, Inc.: Wallingford CT, **2010**.
- (S2) Hong, D.; Tsukakoshi, Y.; Korani, H.; Ishizuka, T.; Kojima, T. Visible-Light-Driven Photocatalytic CO₂ Reduction by a Ni(II) Complex Bearing a Bioinspired Tetradentate Ligand for Selective CO Production. *J. Am. Chem. Soc.* **2017**, *139*, 6538–6541.
- (S3) Yang, J.; Weng, L. Zheng, H. Alternative Synthesis of 1,2,3,4-Tetramethoxy-5-methylbenzene: A Key Intermediate for Preparing Coenzyme Q Homologs and Analogs. *Synthetic Communications* **2006**, *36*, 2401–2405.
- (S4) Nakagawa, T.; Okamoto, K.; Hanada, H.; Katoh, R. Probing with Randomly Interleaved Pulse Train Bridges the Gap between Ultrafast Pump-Probe and Nanosecond Flash Photolysis. *Opt. Lett.* **2016**, *41*, 1498-1501.
- (S5) Hathchard, C. G.; Parker, C. A. A New Sensitive Chemical Actinometer. II. Potassium Ferrioxalate as a Standard Chemical Actinometer. *Proc. Roy. Soc. A* **1956**, *235*, 518-536.
- (S6) Chandrasekharam, M.; Rajkumar, G.; Rao, C. S.; Suresh, T.; Reddy, M. A.; Reddy, P. Y.; Soujanya, Y.; Bessho, T.; Jun-Ho, Y.; Nazeeruddin, M. K.; Grätzel, M. Polypyridyl Ru(II)-sensitizers with extended π -system enhances the performance of dye sensitized solar cells. *Synthetic Metals* **2011**, *161*, 1098–1104.
- (S7) Damrauer, N. H.; Boussie, T. R.; Devenney, M.; McCusker, J. K. Effects of Intraligand Electron Delocalization, Steric Tuning, and Excited-State Vibronic Coupling on the Photophysics of Aryl-Substituted Bipyridyl Complexes of Ru(II). *J. Am. Chem. Soc.* **1997**, *119*, 8253–8268.
- (S8) Ghosh, D.; Takeda, H.; Fabry, D. C.; Tamaki, Y.; Ishitani, O. Supramolecular Photocatalyst with a Rh(III)-Complex Catalyst Unit for CO₂ Reduction. *ACS Sustainable Chem. Eng.* **2019**, *7*, 2648–2657.